# Inhibition underlies fast undulatory locomotion in *C. elegans*


- Author names and affiliations, including postal codes.
  Lan Deng[1], Jack Denham[2], Charu Arya[1], Omer Yuval[2], Netta Cohen[2], Gal Haspel[1]

  [1]Federated Department of Biological Sciences, New Jersey Institute of Technology and Rutgers University, Newark NJ USA, 07032;
  [2]School of Computing, University of Leeds, Leeds, LS2 9JT UK

- Corresponding author email address
  haspel@njit.edu


- Number of pages
  31

- Number of figures, tables, multimedia, and 3D models (separately)
  8 figures, 5 extended data tables

- Number of words for abstract, introduction, and discussion (separately)
  Abstract 239, Introduction 651, Discussion 1500

- Conflict of interest statement
  The authors declare no conflicts of interest.


- Acknowledgments

  LD thanks her thesis committee: Farzan Nadim, Daphne Soares, Andrew Leifer, and Eric Fortune for useful discussions, encouragement, and support. JED and NC thank Thomas Ranner for useful and critical discussions. Some strains were provided by the CGC, which is funded by the NIH Office of Research Infrastructure Programs (P40 OD010440).We also thank the National Bioresource Project of Japan, and the Takagi and Nakai Laboratories for providing strains. NC was funded by EPSRC (EP/J004057/1).

***Abstract***

Inhibition plays important roles in modulating the neural activities of sensory and motor systems at different levels from synapses to brain regions. To achieve coordinated movement, motor systems produce alternating contraction of antagonist muscles, whether along the body axis or within and among limbs. In the nematode *C. elegans*, a small network involving excitatory cholinergic and inhibitory GABAergic motoneurons generates the dorsoventral alternation of body-wall muscles that supports undulatory locomotion. Inhibition has been suggested to be necessary for backward undulation because mutants that are defective in GABA transmission exhibit a shrinking phenotype in response to a harsh touch to the head, whereas wild-type animals produce a backward escape response. Here, we demonstrate that the shrinking phenotype is exhibited by wild-type as well as mutant animals in response to harsh touch to the head or tail, but only GABA transmission mutants show slow locomotion after stimulation. Impairment of GABA transmission, either genetically or optogenetically, induces lower undulation frequency and lower translocation speed during crawling and swimming in both directions. The activity patterns of GABAergic motoneurons are different during low and high undulation frequencies. During low undulation frequency, GABAergic VD and DD motoneurons show similar activity patterns, while during high undulation frequency, their activity alternate. The experimental results suggest at least three non-mutually exclusive roles for inhibition that could underlie fast undulatory locomotion in *C. elegans*, which we tested with computational models: cross-inhibition or disinhibition of body-wall muscles, or inhibitory reset.

***Significance Statement***

Inhibition serves multiple roles in the generation, maintenance, and modulation of the locomotive program and supports the alternating activation of antagonistic muscles. When the locomotor frequency increases, more inhibition is required. To better understand the role of inhibition in locomotion, we used *C. elegans* as an animal model, and challenged a prevalent hypothesis that cross-inhibition supports the dorsoventral alternation. We demonstrate via behavior analysis that inhibition is related to speed rather than the direction of locomotion and that it is unnecessary for muscle alternation during slow undulation in either direction but crucial to sustain rapid dorsoventral alternation. We used calcium imaging of motoneurons and muscle as well as computational models to test hypotheses for the role of inhibition in locomotion.

## Introduction

Alternating activation of antagonistic muscles is ubiquitous in motor programs. During locomotion, limbed animals alternate flexor–extensor muscles as well as their left and right counterparts, while limbless locomotion involves antagonistic axial muscles that generate body bending. The generation of an alternating pattern often involves direct or indirect inhibitory pathways to the antagonistic motoneuron pool (Kiehn, 2011, 2016). Inhibition serves multiple roles in the generation, maintenance, and modulation of the locomotive program. Hypotheses range from cross-inhibitory induced alternation of antagonists to postinhibitory rebound contributing to rhythm generation. Ascending interneurons produce recurrent inhibition of sensory pathways that gate reflex responses and limit firing of central pattern generator (CPG) neurons, while descending interneurons can produce tonic or phasic inhibition that reduces responsiveness and spontaneous locomotion, or stop it all together (Roberts *et al*., 2008). Negative regulation plays a role in modulating performance of parts to overall speed-up processes of complex systems in very disparate fields, from evolutionary adaptation and ecology to pedestrian and vehicle traffic (Gershenson and Helbing, 2015), and genetic networks. For example, negative autoregulation of gene networks, in which a gene product plays as a repressor of their transcription, speeds-up the response time of gene circuits, while also promoting robustness (Alon, 2007).

In *C. elegans*, GABAergic motoneurons have been suggested, based on their morphology, connectivity, and mutant phenotype, to provide cross-inhibition necessary for backward crawling (McIntire *et al*., 1993a; McIntire *et al*., 1993b; Schuske *et al*., 2004). The locomotion circuit is composed of 75 motoneurons, divided by their morphology into 4 excitatory cholinergic and 4 inhibitory GABAergic classes that innervate 95 body-wall muscles. The motoneurons synapse onto thin processes called muscle arms that are extended from muscle cells onto the ventral cord (White *et al*., 1976, 1986; Chen *et al*., 2006; Emmons, 2015; Altun and Hall, 2009). Muscle arms are functionally analogous to vertebrate motoneurons, while *C. elegans* motoneurons are functionally analogous to vertebrate spinal interneurons. GABAergic inhibitory motoneurons (namely 6 DD and 13 VD that innervate dorsal and ventral muscles, respectively) receive inputs only from other motoneurons (White *et al*., 1976, 1986; Haspel and O'Donovan, 2011; Petrash *et al*., 2013). Each VD receives input from the dorsal cholinergic motoneurons (DA, DB, and AS) that innervate the opposing muscle cells, while DD motoneurons receive input from the ventral cholinergic motoneurons (VA and VB) (White *et al*., 1976, 1986; Haspel and O'Donovan, 2011). In addition to their synaptic output at neuromuscular junctions, opposing DD and VD motoneurons also innervate each other, whereas VD motoneurons also innervate the local VA and VB (Fig. 8a) (White *et al*., 1986; Haspel and O'Donovan, 2011).

Mutant strains of *C. elegans* that are defective in any part of their GABAergic transmission (the so-called *shrinker* mutants) respond to anterior noxious stimuli, such as a harsh touch to the head, with coactivation instead of alternation of antagonistic dorsoventral muscle, producing a shrinking response instead of the rapid reverse undulation seen in the wild type. The mutant animals as well as animals with laser-ablated GABAergic motoneurons, shorten the anterior portion of their body and have been reported not to move backward while performing normal forward crawling, albeit with decreased undulatory amplitude (McIntire *et al*., 1993a; McIntire *et al*., 1993b). Hence, it was suggested that GABAergic motoneurons mediate dorsoventral cross-inhibition during backward locomotion (McIntire *et al*., 1993b), or direction change (Schuske *et al*., 2004). According to this hypothesis, when an excitatory cholinergic A motoneuron (e.g., VA) activates postsynaptic muscle arms, it also activates an inhibitory GABAergic motoneuron (e.g.,

DD) that prevents excitation of the opposing muscle; shrinking may be caused by the coactivation of dorsal and ventral A motoneurons, or by coactivation by A- and B-type motoneurons. An alternative hypothesis suggests that neural, rather than muscular inhibition, plays an important role (Boyle *et al*., 2012). In a computational model testing this hypothesis, abolishing neural inhibition from VD to VB is detrimental to rapid but not for slower undulation.

Here, to assess the relative contributions of these hypotheses, we quantified the response to harsh touch and spontaneous crawling and swimming behaviors of different GABA transmission mutants as well as an optogenetic strain in which GABAergic motoneurons can be inactivated acutely. We recorded the activity of GABAergic motoneurons with calcium imaging during low and high undulation frequencies. Finally, we suggested competing hypotheses for the roles of inhibition in *C. elegans* locomotion and tested them with computational models.

## Methods

*C. elegans strains.* We maintained *C. elegans* strains under standard laboratory conditions on Nematode Growth Medium (NGM) agar plates with OP-50-1 *Escherichia col*i (*E. coli*) bacterial lawn at 20°C (Brenner, 1974; Corsi *et al*., 2015). All animals used in the experiments were hermaphrodites.

The *C. elegans* strains used in this study were N2, VC1433, TM5916, TM5487, CB1562, CB120, TOL12, TOL15, TOL11, and CZ1632. We obtained N2 (a reference laboratory strain considered as wild type), VC1433 *[unc-25 (ok1901) III]*, CB1562 *[vab-7(e1562) III]*, CB120 *[unc-4(e120) II]*, and CZ1632 (*juIs76 [unc-25p::GFP + lin-15(+)]II*) strains from the Caenorhabditis Genetic Center of University of Minnesota (https://cgc.umn.edu/), and TM5916 *[unc-46 (tm5916)]V* and TM5487 *[unc-49 (tm5487)]III* from the National Bioresource Project of Japan (https://shigen.nig.ac.jp/c.elegans/top.xhtml). We generated TOL11 (*aatIs11[myo-3p::R-CaMP2; unc-25p::G-CaMP6; unc-47p::ChR2::P2A::DsRed2; odr-1p::DsRed]III* and TOL12 (*aatIs12[unc-47p::Arch::GFP, myo-2p::mCherry*]) by integrating the extrachromosomal arrays in *jqEx456 [myo-3p::R-CaMP2; unc-25p::G-CaMP6; unc-47p::ChR2::P2A::DsRed2; odr-1p::DsRed](Inoue et al., 2015),* and OKA074 (*ncEx2351 [unc-47p::Arch::gfp, myo-2p::mCherry]*) (Okazaki *et al*., 2012) into the animals' genome via UV irradiation methods, respectively; then we crossed the integrated strains with wild type N2 for at least 5 generations and screened for the homozygous (Ahringer, 2006). We generated TOL15 by crossing TOL14 (*aatIs4 [myo3p::nls::RCaMP2]V*) and ZW495 (*zwIs132 [myo-3p::GCamp2 + lin-15(+)]*) and screening for homozygotes for *aatIs4* and *zwIs132*.

*Free locomotion behavioral tracking.* We recorded the free crawling and swimming of wild type, GABA transmission knockouts, and an optogenetic strain on NGM agar plates or in NGM buffer solution using a static multi-worm tracker. The tracker was composed of three major parts. From top to bottom, a camera (Basler ace acA4024-29um) connected to a fixed focal length lens (C Series 5MP 35mm 2/3" fixed focal length lens, Edmund Optics) with an infrared cut-off filter (M25.5x0.5 Mounted IR Cut-Off Filter, Edmund Optics), a specimen stage for plates or slides, and an infrared LED light (M850L3, Thorlabs) mounted with a collimation adaptor (COP1-B-Collimation Adaptor, Thorlabs).

One day before recording, we transferred fourth larval stage (L4) animals onto new NGM plates with OP-50-1 *E. coli* bacterial lawn so that experimental animals would be first-day young adults. During tracking, at least 30 animals were freely moving on 35 mm NGM plates without

bacterial lawn or in NGM solution between a microscope slide and a coverslip, 1 mm apart. We recorded at least 9 videos with Pylon Viewer (Basler pylon Camera Software Suite) at 25 frames per second (fps) for 15 to 20 s. During video acquisition, we cropped the video frame dimensions to approximately 2,000x2,000 pixels.

One day before behavioral tracking of the optogenetic strain TOL12, we transferred L4 animals onto NGM plates that had been freshly seeded with 50 mM all-trans-retinal (ATR) in OP-50-1 *E. coli*. To allow the animals to incorporate ATR, we kept the plates in the dark at 20°C for 24 h. Animals fed with ATR but recorded in the dark (under infrared LED) were tracked as one negative control group, and the same animals under lime-color LED light that activated Archaerhodopsin-3 were the experimental group. Another negative control group was TOL12 animals not fed with ATR but kept and tracked under the same conditions as the experimental group. The optogenetic strain that not fed with ATR is not responsive to the activation light of the optogenetic protein. We used lime-color light (M565L3, 565 nm LED with a Collimator), which is the optimal activation light of Archearhodopsin-3 (Mattis *et al*., 2011; Okazaki *et al*., 2012), with a working illumination power of 10 mW/cm$^2$. To prevent desensitization of TOL12 to the activation light, the maximum time of light exposure was 1 m (Okazaki *et al*., 2012). The rest of the operations and software settings were the same as the behavior tracking aforementioned.

*Head and tail harsh touch experiments.* We transferred L4 animals to new OP-50-1 *E. coli*-seeded NGM plates one day before the experiment. During the experiment, we transferred animals onto 60 mm NGM plates without bacterial lawns. We touched the head or tail of the animals using a blunt glass probe while they were crawling forward. We acquired the videos continuously with a CMOS camera (U3CMOS14000KPA, ToupTek) and acquisition software (ToupView, https://www.touptek.com/) at 30 fps and 1,048x822 pixels greyscale during several stimulations of different animals. We further trimmed these videos into clips with one stimulation each by video editing software Premiere Pro (Adobe) or Shotcut (https://shotcut.org/).

*Behavioral tracking analysis.* We processed crawling and swimming tracking using Tierpsy Tracker v1.4.0, a multi-worm behavior tracker software (https://github.com/ver228/tierpsy-tracker/releases/) (Javer *et al*., 2018). Then, we analyzed the processed results in hdf5 files using custom programs written in Matlab.

Each video had between 10 and 30 animals each assigned with an index by Tierpsy. We analyzed the translocation speed and undulation frequency during forward and backward locomotion from the mid-body of the animals as well as primary wavelength and maximal amplitude. Tierpsy computes the undulation frequency using the waveform frequency from the largest peak via the Fourier transform over a time window.

We used Tierpsy Tracker v1.4.0 to extract the aforementioned kinetic parameters from trimmed video clips before and after head or tail stimulation. We calculated the means of these 4 parameters within 5 s before and 5 s after the stimulation from trimmed videos of head and tail stimulation experiments.

*Changes in body length.* We analyzed the body length at different time in the trimmed clips in each stimulation direction of N2 strain and each of the GABA transmission knockout strains, as well as head stimulation of *vab-7* mutant animals (CB1562) and tail stimulation of *unc-4* mutant animals (CB120): before the harsh stimulation, immediately after the stimulation, as well as 0.5 s, 1 s, and 2 s after the stimulation. We used 'Freehand Line' tool in ImageJ (https://imagej.nih.gov/ij/) to

measure the body length of animals. We expressed the body length as the percentage of pre-stimulus length and plotted the means of normalized body lengths for each strain at each time point.

*Calcium imaging in a microfluidic device.* To repeatedly measure activity at particular phases of the locomotor cycle, we placed young adult animals in a waveform silicon microfluidic device with channels designed to restrict their motion to a pattern that mimics undulatory locomotion. The cycle was fixed in space and predictable at any location along the path (Fig. 7a). The wavelength, amplitude, and width of the channel were 686.5, 322.5, and 133.5 µm, respectively. To unify the frame of reference, we arbitrarily designated the phase of a maximal dorsal bend as 90° and a maximal ventral bend as 270° (Fig. 7a) and defined the rest of the phase positions accordingly. We presented collated recordings during forward locomotion from motoneurons and body-wall muscle with phase (rather than time) being the common frame of reference.

We transferred healthy fourth larval stage (L4) animals to new plates seeded with OP-50-1 *E. coli* one day before imaging. We added drops of methyl cellulose solution onto the face of a microfluidic device, and then transferred the animals into these drops. To seal the microfluidic device, we flipped covered it with an 18 mm diameter round coverslip, flipped the coverslip so the device is on top for the inverted microscope and sealed by pressing on the device. The transgenic animals could crawl freely inside the channels, and we manipulated their undulation frequency by changing the ambient viscosity. We used 3% and 0.5% (w/w) methyl cellulose in NGM buffer while recording calcium level changes in GABAergic motoneurons in TOL11, 1.5% (w/w) methyl cellulose to record calcium level changes in body-wall muscles in TOL15, and 3% and 0.5% (w/w) methyl cellulose to image GFP (as a negative control calcium-insensitive fluorescent protein to determine motion artifact) in GABAergic motoneurons in CZ1632. We only recorded calcium level changes in animals that moved smoothly in the microfluidic channel.

To image and record the fluorescence change of GCaMP or GFP, we used an inverted microscope (Olympus IX73) with a 40x/NA0.95 UPlanSApo objective and an sCMOS camera (Hamamatsu Orca Flash 4.0) and a solid-state excitation light source (X-Cite 120LED) with a dual-band filter set (Chroma 59022 ET-EGFP/mCherry), and a dual camera image splitter (TwinCam, Cairn Research with a T565lpxr dichroic beam splitter). We used Micro-Manager (v1.4; https://micro-manager.org/) to acquire multiple videos of animals moving through different parts of the channel (i.e., different locomotor phases). We saved videos as separate tiff files (2,048x2,048 pixel resolution) at a frame rate of 100 fps with 10 ms exposure for animals crawling in 0.5% (w/w) methyl cellulose, and 50 fps with 20 ms exposure for animals crawling in 1.5% (w/w) and 3% (w/w) methyl cellulose. We did not use NGM with less than 0.5% (w/w) methyl cellulose because it resulted in discontinuous and less smooth locomotion. Between acquisitions, we moved the microscope stage manually to follow animals when they moved out of view. We in muscle cells and motoneurons in the mid-body: dorsal muscle cells 9-21(n=24), ventral muscle cells 9-21(n=27), DD motoneurons 2-5 (n=26), VD motoneurons 3-10 (n=59).

We used a customized Matlab program (available on GitHub) to analyze the change in fluorescence intensity inside the identifiable body-wall muscle cells or somata of GABAergic motoneurons. For each frame, we measured the mean fluorescence intensity of the top 50% pixels within the manually traced region of interest (ROI) around the cell of interest ($F_{top50\%}$). We then calculated and subtracted the median intensity of the frame as the background ($F_{BG}$). Finally, we demeaned the value by dividing it by the mean fluorescence signal of this cell in this video of n frames: $\Delta F/F = (F_{top50\%}-F_{BG}) / (\Sigma(F_{top50\%}-F_{BG})/n)$. Our Matlab code provides a graphical user

interface (GUI) to track the cell as it moves across the field of view, following a trajectory that is set by the waveform channel, to mark the location of 90° (maximal dorsal bend) or 270° (maximal ventral bend, Fig. 7a), and to trace ΔF/F against time or undulatory phase. We categorized traces from GABAergic motoneurons into low- and high-frequency (with 0.6 Hz as cut-off, see results) undulations of crawling inside the microfluidic channel; the undulation frequency was calculated as the fraction of locomotor cycle traveled by the cell of interest divided by the elapsed time. We collated and plotted all traces of ΔF/F against the phase of each type of cell at 5° bins. We corrected the soma position of motoneurons to their neuromuscular postsynaptic position according to the published perimotor locations (Chen *et al*., 2006; Haspel and O'Donovan, 2011). We removed videos or parts of videos in which the cell of interest went out of focus or if we could not positively identify it.

*Computational modeling.* We use an integrated neuromechanical model consisting of a mechanical body, driven by neuromuscular activation, and subjected to fluid drag forces (Denham *et al*., 2018), thus allowing us to probe different hypotheses about neural control and test their consequences in different fluid environments. We chose to focus on control circuits for only one direction of locomotion, an assumption that follows from our own results that suggest that the phenotypes of the GABA transmission mutant are manifested not only during a switch in direction, but also during forward and backward locomotion and primarily caused by defects in the ventral nerve cord circuitry, rather than by defects in premotor interneurons. To this end, we adapted an existing model of forward locomotion control (Denham *et al*., 2018). In particular, we explored two different forms of neural control: a proprioceptively driven model and a feedforward model, mimicking CPG control (Denham *et al*., 2018). We subjected each model to different perturbations and explored the behavior generated in our neuromechanical framework in liquid and agar-like conditions. For the model equations and parameters, see the Supplementary Materials (see also https://bitbucket.org/leedswormlab/curve-worm-inhibition-paper. Both models of neural control output a single muscle activation function acting continuously along the body, which sums the muscle activation from cholinergic B-type excitatory and GABAergic D-type inhibitory motoneurons on both sides of the body (Fig. 8b). Our approach to modeling is parsimonious, with the aim of maximizing the explanatory power of the model with respect to the specific model hypotheses, and specifically about the effect of inhibition on undulation frequency. Therefore, differences in dorsal versus ventral activation (Piece-Shimomura, 2008), detailed muscle anatomy (e.g. around the pharynx and vulva), more detailed representations neural connectivity (Haspel and O'Donovan, 2011), cuticle viscosity, models of muscle tone modulations, variations of the neural circuit or muscle properties along the anterior-posterior axis, and rigorous models of the external fluid dynamics, are all neglected in this study.

*Proprioceptive Control.* In *C. elegans*, proprioceptive control of forward locomotion is mediated by B-type excitatory motoneurons (Wen *et al.,* 2012, Fouad *et al*., 2018). In or model, B-type motoneurons receive proprioceptive input, which corresponds to the mean body curvature integrated over their receptive range, set here to half the body length, posteriorly to the muscle coordinate (Denham *et al*., 2018). Excitatory ventral B-type (VB) and dorsal B-type (DB) motoneurons act as bistable switches, at every point along the body. Each switch is associated with two thresholds (for switching on and off, akin to Boyle *et al.* 2012). Premotor activation from AVB is absorbed into the thresholds for parsimony. Following Boyle *et al*. (2012) and the published connectivity (Chen et al 2006), we also assumed D-type neurons instantaneously react to excitation from B-type neurons on the opposite side of the body (Fig. 8a). Thus, if DB (or VB) is on at some

point along the body, VD (or DD) is activated. In addition, we include VD-to-VB inhibition (Fig. 8a), with the inhibition strength set such that the thresholds of VB and DB collapse to a single bistable switch when DB (hence also VD) is active. The corresponding reduced model, with only a single bistable switch, is presented and analyzed in depth in Denham, Ranner & Cohen (2018). In particular, this model qualitatively captures external gait modulation due to the coupling between neural control and biomechanics (measured in terms of the dependence of the frequency and waveform of undulations on the external viscosity of the fluid). Due to the simplifications above, the model does not predict precise waveforms.

*CPG control*. Following Denham *et al.* (2018) and in the absence of detailed CPG mechanisms, we modeled the essential feature of feedforward control, namely the existence of endogenous, central pattern generation that produce neural oscillations at a characteristic frequency and is embedded in a biomechanical body. We therefore model the neural activation, $A(u,t)$, at location, u, and time, t, by a retrograde traveling sine wave that activates the muscles continuously along the body: $A(u,t) = sin(2\pi uL/\lambda_{\mathrm{f}} - 2\pi t/T_{\mathrm{f}})$, where $L$ is the body length, and $\lambda_{\mathrm{f}}, T_{\mathrm{f}}$ are the wavelength and period of the undulation.

*Model muscles.* Under proprioceptive control, the neural circuit controls the muscles, modeled by a leaky integration equation that converts the muscle activation function at every point along the body, $u$, to a mechanical torque. The muscle model contains two free parameters, corresponding to a muscle time scale (100 ms in the wild type) and an amplitude or maximum curvature (10 $\mathrm{mm}^{-1}$ in the wild type, see Denham *et al.* (2018) for discussion). In the CPG-driven model, we modeled the effect of muscle disinhibition by sharpening the rise in muscle activation using a hyperbolic tangent function (Supplementary materials), which we removed when accommodating our muscle disinhibition hypothesis (see Model perturbations section below).

*Biomechanics.* Our model of the *C. elegans* body consists of a continuous incompressible viscoelastic shell. At each point along the body, we assumed the radius of the nematode's body is fixed in time, which allows us to collapse all internal and external forces onto the midline (Denham *et al*., 2018; Ranner, 2020). Four free parameters modulate the biomechanical properties of the body and its interaction with the environment. Environmental forces were modeled by resistive force theory and parametrized by two drag coefficients that act to resist the motion in the normal and tangential directions (Berri *et al.*, 2009, Boyle *et al.*, 2012, Denham *et al.*, 2018). This allows us to model both Newtonian and linear viscoelastic environments in the low Reynolds number regime. Our simulations here mimic two environmental conditions: swimming in liquid (buffer solution) and crawling on agar. The passive body is parametrized by Young's modulus (the effective elastic resistance to bending or body stiffness, set to 100 kPa for the wild type), and an internal viscosity (the body damping in response to bending), which we neglect for simplicity. The model equations balance internal and external forces and torques subject to mass conservation within the nematode's body and an inextensibility closing constraint (Cohen and Ranner, 2017; Ranner, 2020).

*Model perturbations:*

*1. Eliminating cross-inhibition of opposing body wall muscles (Hypothesis 1).* To implement this hypothesis, we eliminated all muscle inhibition by D-type neurons, leaving neural inhibition intact. In our model, the muscle forcing on both sides of the body is combined into a single muscle activation function acting along the midline of the body. Therefore, the elimination of muscle cross-inhibition by D-type neurons is equivalent to decreasing the effective excitation by the actively contracting side of the body. Unless otherwise stated, we set the strength of the muscle inhibition by D-type neurons to 20% that of the muscle excitation by B-type neurons (estimating

that animals with maximal shrinking are at most 20% shorter than in the fully relaxed state, see discussion in Supplementary Materials section S1 and parameter sweep in Fig. S1).

*2. Eliminating disinhibition of innervated body wall muscles (Hypothesis 2).* This could be modeled by a more complex nonlinear muscle model. Alternatively, using our linear muscle model, we assumed a faster muscle response following phasic release from inhibition. In the proprioceptive model, this is achieved by reducing the muscle time scale and therefore crudely models the faster response by alternating sides of the body. Unless otherwise stated, we increased the muscle time scale by 20% to mimic the effect of eliminating the disinhibitory muscle response (for parameter sweep, see Supplementary Fig. S1). In the CPG-driven wild-type model, we model a faster muscle response by sharpening the increase and decrease in our periodic muscle activation using a hyperbolic tangent function, $\beta_0 \tanh\big(\alpha A(u,t)\big) / \tanh(\alpha)$, keeping the amplitude, $\beta_0$, unchanged. The tanh function is either entirely omitted to mimic the extreme perturbation (the default perturbation), or gradually suppressed (through a modulation of $\alpha$) in parameter sweeps (Fig. S1).

*3. Eliminating inhibitory reset of VB by VD (Hypothesis 3).* In our proprioceptive control model, elimination of neural inhibition implies that VB neurons are not inhibited when DB neurons are active, but that muscle inhibition remains intact. Thus, we modeled this perturbation by a constant positive offset applied to both thresholds of the VB bistable switch. Since our sinusoidal feedforward model does not take into account individual motoneurons, we only explore this hypothesis in the feedback model.

In coordinated locomotion, the undulation frequency (the reciprocal of the period of undulation) was computed from curvature kymograms. For a given point along the body, the period was defined as the mean time interval between positive (increasing) zero crossings of the body curvature.

*Experimental design and statistical analysis.* For free crawling behavior tracking of N2 (wild type), the number of videos, animals, and data points were 12, 235, and 67,209, respectively, for VC1433, the numbers were 11, 213, and 80,407; for TM5916 the numbers were 11, 255, and 94,446, and for TM5487 the numbers were 12, 289, and 121,374. For free swimming behavior tracking of N2 (wild type), the numbers of videos, animals, and data points were 46, 707, and 164.057, respectively, for VC1433, the numbers were 39, 778, and 247,656; for TM5916 the numbers were 38, 1014, and 316,094; and for TM5487, the numbers were 34, 668, and 293,482. For free crawling behavior tracking of TOL12 without ATR feeding, the number of videos, animals, and data points were 20, 375, and 104,098, respectively. For TOL12 that were fed with ATR and tracked in the dark, the numbers were 27, 335, and 98,017; and for TOL12 that were fed with ATR and were exposed to lime light during tracking, the numbers were 26, 235, and 66,803. For free swimming behavior tracking of TOL12 without feeding ATR, the number of videos, animals, and data points were 20, 326, and 81,291, respectively. For TOL12 that were fed with ATR in advance and tracked in the dark the numbers were 22, 361, and 97,630; and for TOL12 that were fed with ATR and were exposed to lime light during tracking, the numbers were 18, 216, and 48,323. We collated the means of these parameters from individual animals from all the videos, and then used one-way ANOVA and Tukey's multiple comparison to compare the estimated population means among strains or different conditions.

For the head and tail harsh touch experiments, we obtained 9 trimmed videos for each stimulation direction for N2 and GABA transmission knockout strains (VC1433, TM5916, TM5487) as well as 9 trimmed videos for *vab-7* mutants (CB1562) of head harsh touch and *unc-4*

mutants (CB120) of tail harsh touch. We used a paired two-tail t-test to determine statistical differences in the parameters before and after stimulation of the same strain, and one-way ANOVA and Tukey's multiple comparison for the parameters of after harsh touch to the head or tail between wild-type and other mutant strains, including GABA transmission knockouts, and *vab-7* and *unc-4* mutants.

To generate linear regressions of sinusoidal crawling and swimming behaviors, we first picked the data points where the primary or secondary wavelengths could be extracted by the analysis software (Tierpsy). These data points in crawling behavior were 4% to 23% of the raw data. The sample sizes of wild type, *unc-25, unc-46*, and *unc-49* during forward crawling were 11,935 (23%), 7,760 (14%), 7,773 (12%), and 5,378 (7%), respectively, those during backward crawling were 1,260 (11%), 2,319 (11%), 2,552 (10%), and 1,714 (4%), respectively. The data points in swimming behavior were 6% to 54% of the raw data. The sample sizes of wild type, *unc-25, unc-46,* and *unc-49* during forward swimming were 74,948 (54%), 46,355 (26%), 69,682 (31%), and 17,015 (11%), respectively, those during backward swimming were 2,137 (14%), 6,249 (11%), 16,728 (21%), and 7,297 (6%), respectively. Then, we picked the data points where the path of an undulation cycle (translocation speed × undulation cycle period) was larger than either the primary or secondary wavelength. Based on this selection criterion, we picked 27 to 54% data points for the correlation construction in crawling behavior. The sample sizes of wild type, *unc-25, unc-46*, and *unc-49* during forward crawling were 5,671 (48%), 2,058 (27%), 2,259 (30%), and 2,313 (43%), respectively, those during backward crawling were 686 (54%), 1,096 (47%), 1,199 (47%), and 856 (50%), respectively. We picked 0.4% to 26% data points in swimming behavior. The sample sizes of wild type, *unc-25, unc-46*, and *unc-49* during forward swimming were 271 (0.4%), 3,985 (14%), 2,086 (3%), and 2,965 (17%), respectively, those during backward swimming were 138 (7%), 1,150 (18%), 975 (6%), and 1,897 (3%), respectively. Using these selected data, we calculated linear regressions between undulation frequency and translocation speed in forward and backward crawling and swimming separately.

For the calcium imaging experiment, we included data analyzed from 11 focused and cell-identifiable videos of TOL15; 11 and 9 videos of CZ1632, TOL11 in 0.5% (w/w) methyl cellulose, respectively, and 12 and 9 videos in 3% (w/w) methyl cellulose, respectively. From these videos, we analyzed 27 and 24 ventral and dorsal body-wall muscles, respectively, in TOL15; 17 VD and 18 DD motoneurons in the high undulation frequency and 26 VD and 13 DD motoneurons in low frequency in CZ1632; and 32 VD and 15 DD motoneurons in the high undulation frequency and 27 VD and 14 DD motoneurons in low frequency in TOL11.

## Results

### Both wild-type and GABA transmission mutants shrank in response to harsh touch to the head or tail

*C. elegans* mutants defective in GABA transmission are known as '*shrinkers*' because of their distinct decrease in body length in response to a harsh touch to the head (McIntire *et al*., 1993a; McIntire *et al*., 1993b; Schuske *et al*., 2004), to which wild-type animals respond with rapid backward motion. Because this phenotype has been described as a defect in backward locomotion, we first looked at the shrinking response of wild-type and GABA transmission mutant animals to harsh touch to the head, which induces rapid backward undulation in wild-type animals as well as the response to the tail touch to study the association of shrinking response to forward locomotion.

We chose three knockout mutant strains in which hundreds to thousands of DNA base pairs had been deleted in the genes encoding the GABA synthesis enzyme glutamic acid decarboxylase (GAD, *unc-25*, VC1433), vesicular transporter (*unc-46*, TM5916), and ionotropic GABA receptor (*unc-49*, TM5487), and compared them to the laboratory reference strain (wild type, N2). We found that the shrinking response was common in wild-type and mutant animals following head or tail stimulation (Fig. 1a). To quantify the shrinking response of wild-type and the GABA transmission knockout animals, we measured the change in body length for each strain and stimulation direction (n=9 each) at four different times (before, immediately after, 0.5 s, and 2 s after stimuli), and normalized the body length to their value before stimuli (Fig. 2a, Table 2-1). Immediately after a harsh touch to the head or tail, both wild-type and the GABA transmission knockout animals decreased their body length, while wild-type animals shrank less: the body length of wild-type animals reduced to 94% ± 2% and 95% ± 3% (mean ± SD), respectively, while the body length of GABA transmission knockouts was reduced to 90–92% ± 2–4%. In addition, wild-type animals recovered to their pre-stimulus body length faster. At 2 s after the head and tail stimulation, the body length of wild-type animals reached to 98–99% ± 2–4% of the pre-stimulus body length, while that of the mutants was 92–97% ± 4–6%.
Moreover, GABA transmission knockouts occasionally exhibited spontaneous shrinking (Fig. 1f). [Spontaneous shrinking in N2 with and without frequency change]

A possible explanation for the dorsoventral coactivation of body-wall muscle that causes body shrinkage in response to harsh touch is the simultaneous activation of all A- and B- type cholinergic motoneurons by premotor interneurons that are associated with forward and backward locomotion. These distinct groups of interneurons activate either DA and VA motoneurons during backward, or DB and VB motoneurons during forward locomotion (Haspel *et al*., 2010). This hypothesis requires a short temporal overlap of activation of A- and B-type cholinergic motoneurons. To test this hypothesis, we took advantage of developmental phenotypes that render mutants in a complementary pair of homeodomain transcription factors (UNC-4 and VAB-7) lacking either A- or B-type motoneurons. In *unc-4* mutant animals (CB120), cells destined to be A-type motoneurons differentiate as B-type motoneurons and receive input from forward-associated premotor interneuron (Miller *et al*., 1992; Miller and Niemeyer, 1995). While it is unclear whether the misdifferentiated neurons fully function as B-type motoneurons, their function as A-type is impaired. Consequently, only their backward locomotion in uncoordinated. Hence, we tested whether *unc-4* mutant animals shrink in response to harsh touch to the tail that induces an acceleration forward, towards their unaffected direction. Correspondingly, in *vab-7* mutant animals (CB1562), cells destined to be DB motoneurons differentiate as DA motoneurons (Esmaeili *et al*., 2002). Consequently, only their forward locomotion in uncoordinated. Hence, we tested whether *vab-7* mutant animals shrink in response to harsh touch to the head that induces an acceleration towards their unaffected direction. The harsh touch stimuli induced a brief reducetion of body length in animals of both mutant strains (Fig. 2a) that was not different from that of the wild type (one-way ANOVA with Tukey test, *Vab-7*: p=0.124, 0.975, 0.974, 0.950; *unc-4:* p=0.963, 0.999, 0.998, 0.892; pairwise comparison of percent of pre-stimulus to wild type immediately after, 0.5 s, 1 s, and 2 s after stimuli; Table 2-1). These results are inconsistent with the hypothesis of coactivation by premotor interneurons, suggesting instead that the shrinking phenotype is localized within the VNC motor circuit and not associated with directional change.

**GABA transmission knockouts failed to escape as rapidly as wild type after harsh touch stimulation**.

After harsh touch stimulation, wild-type animals were able to escape at high frequency and translocation speed, while the mutants moved away slowly (Fig. 1a, note location at 5 s). We measured the translocation speed and midbody undulation frequency as well as the maximal amplitude and primary wavelength, within 5 s before and 5 s after stimulation (n=9 video clips for each strain and stimulation location, Fig. 2b, Tables 2-2 and 2-3). After harsh touch to the head or tail, wild-type animals escaped with significantly higher translocation speed and undulation frequency, while GABA transmission knockouts had lower mean translocation speeds except for *unc-46* and *unc-49* after harsh tail touch, and lower mean undulation frequency, except for *unc-49* after harsh tail touch. Compared to the locomotion within 5 s after the harsh head or tail touch of the wild type, all the GABA transmission knockouts had significantly lower translocation speed (one-way ANOVA with Tukey test, $p < 0.0001$ pairwise comparison to wild type) and undulation frequency ($p < 0.05$ pairwise comparison to wild type; Fig. 2b, Table 2-3). Wild-type and GABA transmission knockouts exhibited larger amplitudes, but unchanged wavelengths after stimulation statistically (except for *unc-46* after tail harsh touch, Fig. 2b, Table 2-2). Note that to quantify the shrinking response, we chose assays in which animals (including mutants) produced sinusoidal crawling before harsh touch. A possible bias from this selection underestimates the actual differences among strains.

**Defect in GABA transmission resulted in slow locomotion during free crawling and swimming**

Early descriptions of the locomotion defect of GABA transmission mutants and animals in which most GABAergic motoneurons have been laser-ablated emphasize the absence of backward locomotion (McIntire *et al*., 1993b; Yanik *et al*., 2004). However, we noted that GABA transmission knockout strains seem to crawl at low undulation frequencies in both directions, and their locomotion was more impaired during swimming in liquid (consistent with Boyle et al. (2012)). Moreover, shrinking is not unique to backward locomotion but occurs in both mutants and wild-type animals regardless of direction. We recorded and compared unstimulated free crawling and swimming behaviors of wild-type and GABA transmission knockout strains as well as an optogenetic strain (TOL12) in which GABAergic motoneurons can be inactivated acutely by light.

Crawling on the NGM agar surface without bacterial lawn, GABA transmission knockout strains crawled slowly. The distribution of translocation speeds and frequencies of GABA transmission knockouts during forward and backward crawling were significantly different from those of the wild type (KS test, $p < 0.0001$, for *unc-25, unc-46*, and *unc-49*). The wild-type distribution of undulation frequency was bimodal for both forward and backward crawling. The undulation frequency during forward crawling fits two Gaussian distributions: a rapid distribution with 0.84 mixing proportion has a mean value of 0.47 Hz, and a slow one with 0.16 mixing proportion has a mean value of 0.17 Hz (Fig. 3a). GABA transmission knockout strains crawled at lower mean translocation speed and mean undulation frequency compared to the wild type (Fig. 3, Table 3-1). Only the mean undulation frequency of VC1433 during forward crawling was not significantly lower than that of the wild type. The maximal amplitudes and primary wavelength of GABA transmission knockouts were significantly smaller than those of the wild type.

During swimming, *C. elegans* undulates at higher frequencies, wavelengths, and amplitudes (Karbowski *et al*., 2006; Pierce-Shimomura *et al*., 2008; Butler *et al*., 2015). If the absence of

GABA transmission impairs fast undulations, it should have a more severe effect on swimming behavior with a more distinct difference between mutants and wild type. We therefore recorded the swimming behavior of wild-type and GABA transmission knockouts in NGM buffer. Wild-type animals alternated dorsal and ventral bends evenly with larger undulation amplitude and wavelength than during crawling (Fig. 4a1). In comparison, GABA transmission knockouts undulated at a lower frequency with dorsoventral body alternation that was not as symmetric as that of the wild type (Fig. 4a2). The distribution of translocation speeds and frequencies of GABA transmission knockouts during forward and backward swimming were significantly different from those of the wild type (KS test, $p<0.001$; for *unc-25*, *unc-46*, and *unc-49*; Fig. 4b).

Indeed, GABA transmission knockout strains swam at a significantly lower translocation speed and undulation frequency than the wild type (Fig. 4bc, Table 3-1). The maximal amplitudes and primary wavelength of GABA transmission knockouts were significantly smaller than those of the wild type.

The GABA transmission knockout animals are chronically impaired, and the effects we describe on locomotion could rise during development or due to compensation mechanisms. Therefore, we studied the locomotion of a transgenic strain (TOL12) that expresses Archaerhodopsin-3 (Arch3) on the cellular membrane of GABAergic motoneurons, so they can be acutely inactivated by light. Arch3 is a light-sensitive proton pump that requires the cofactor all-trans-retinal (ATR) and causes hyperpolarization when exposed to lime-color light (Nagel *et al*., 2005; Okazaki *et al*., 2012). We fed transgenic animals with ATR for 24 h and tracked their swimming or crawling behaviors under infrared light (that does not activate Arch3) and then under lime-color light, which is the optimal activation wavelength of Arch3 (Mattis *et al*., 2011; Okazaki *et al*., 2012). To prevent desensitization of Arch3 after long exposure, we limited lime-color light to 1 minute (Okazaki *et al*., 2012). We also tracked the locomotion behavior of transgenic animals that were not fed ATR as a negative control. When GABA transmission was inactivated acutely by hyperpolarizing GABAergic motoneurons, the frequency of undulations decreased, comparable to the effect of GABA transmission mutants. Swimming under lime-color light, the transgenic animals fed with ATR were slower and less coordinated, and their maximal amplitude and primary wavelength decreased, but quickly recovered when the optogenetic activation light was turned off (Fig. 5abc). Crawling on agar surface under lime-color light, the translocation speed of transgenic animals fed with ATR was significantly lower than that of the same animals under infrared light and that of the animals not fed ATR under lime-color light. Their undulation frequency was lower than that of the same animals under infrared light and that of the animals not fed ATR. Swimming in NGM buffer, their translocation speed was lower ($p < 0.0001$) than that of the same animals under infrared light and that of the animals not fed ATR. Their undulation frequency was lower ($p < 0.0001$) than that of the same animals under infrared light and that of the animals not fed ATR (Fig. 5d, Table 5-1). In contrast with the swimming of GABA transmission knockout mutants, some data points are as high frequency and fast as in control animals (compare Fig. 4b to Fig. 5c), suggesting an incomplete optogenetic neuronal inactivation.

During free crawling or swimming, *C. elegans* exhibits a variety of behaviors from forward or backward almost-sinusoidal undulations, through omega and delta turns, direction changes, and pauses, to periods of quiescence (Stephens *et al*., 2008). When GABA transmission is impaired by knockout mutations or optogenetic inactivation, *C. elegans* becomes less coordinated, and their undulation frequencies and translocation speed decrease. In order to compare the efficiency of harnessing undulation frequency to produce translocation speed in wild-type and mutant animals, we isolated and analyzed the almost-sinusoidal undulations. For all strains, in both directions of

crawling and swimming, there were positive linear correlations between undulation frequency and translocation speed. Wild type translocated faster with the same undulation frequency compared to any of the GABA transmission knockout strains (Fig. 6ab).

**GABAergic motoneurons showed different activation patterns during low and high undulation frequencies.**

In the absence of GABA transmission, animals did not move at rapid undulation frequency and fast translocation speed in either direction during free locomotion or in response to harsh touch stimulation to the head or tail. However, they were capable of slow dorsoventral undulation in both directions during free locomotion and after stimulation. Moreover, when only sinusoidal undulations are considered, undulation frequency is a predictor of translocation speed in wild-type and mutant animals, with wild type exhibiting higher efficiency. Together, these results suggest that GABAergic motoneurons' contributions depend on undulation frequency and that they are necessary for high-frequency undulation.

To determine the contributions of GABAergic motoneurons during low and high undulation frequency, we recorded their activity with a genetically encoded calcium sensor. We facilitated keeping track of the locomotive phase and undulation frequency by using a silicon microfluidic device with sinusoidal waveform channels designed to mimic the crawling path of wild-type animals (Fig. 7a; Lockery *et al*., 2008). Taking advantage of the predetermined shape of the channel and the published perimotor location of each motoneuron (Chen *et al*., 2006; Haspel and O'Donovan, 2011), we converted the soma position of GABAergic motoneurons during imaging to the locomotive phase of their neuromuscular junction to body-wall muscle. We assigned phases of the locomotion cycle to location in the channel according to the animal's dorsoventral bending and direction of movement. We define the peak of dorsal bending as 90° and that of ventral bending as 270°, with other positions in the channel assigned accordingly. To manipulate the undulation frequency, we changed the viscosity of the fluid inside the channels with increasing concentration of methyl cellulose (in NGM buffer) up to 3% (w/w) methyl cellulose (higher concentrations prevented animals from entering the channels). When animals crawled in 3% (w/w) methyl cellulose, the mean undulation frequency was 0.28±0.14 Hz, which is close to the undulation frequencies of the GABA transmission knockouts during forward crawling (0.32±0.18 Hz, $p = 0.89$). When animals crawled in 0.5% (w/w) methyl cellulose, they could move faster with a mean undulation frequency of 0.74±0.26 Hz, which is above 99.5% of undulation frequency data points obtained in free forward crawling recording (Fig. 6cd). We imaged calcium level changes in the cytoplasm of body-wall muscle cells with GCaMP2 (TOL15) in 1.5% (w/w) methyl cellulose and in the cytoplasm of GABAergic motoneurons with GCaMP6 (TOL11) in 0.5% and 3% (w/w) methyl cellulose. The average undulation frequency in 1.5% methyl cellulose was 0.62±0.20 Hz. Hence, regardless of methyl cellulose concentration, we used 0.6 Hz as the cut-off to categorize data into low and high undulation frequencies. Because *C. elegans* infrequently moved backward in the channels, we only collected and analyzed calcium imaging data for smooth forward locomotion.

The calcium imaging signal from body-wall muscle cells correlated to muscle contraction and bending. The signal increased when ventral muscle cells went through ventral bending (around 270°, Fig. 7b) and when dorsal muscle cells went through dorsal bending (around 90°). During high undulation frequency, GABAergic motoneurons exhibited a sustained level of calcium signal with distinct troughs of phasic low levels (Fig. 7c). VD motoneurons exhibited a phase of low

signal around ventral bending (270°), while DD motoneurons exhibited a corresponding phase of low signal around dorsal bending (90°). Both VD and DD had a phase of low signal around 180˚, and only VD had a rise in calcium signal level between 270° and 360°. In contrast, during low undulation frequency, VD and DD showed the same calcium signal pattern — a wide phase of low signal from 90° to 270° (Fig. 7d). To examine the contribution of movement to the recorded signal, we recorded the change in fluorescence from calcium-insensitive green fluorescent protein (GFP) in GABAergic motoneurons in 0.5% and 3% (w/w) methyl cellulose. Regardless of motoneuron subsets or viscosity conditions, the fluorescence signal of GFP showed a similar pattern: a wide increase in signal from 180° to 360° correlated with ventral bending. Because the fluorescence intensity of GFP is 20-fold brighter than that of GCaMP6, the increase in fluorescence intensity might be due to convergence of fluorescence from neighboring motoneurons when the ventral nerve cord went through ventral bends.

Therefore, GABAergic motoneurons exhibited different patterns of activation during high and low undulation frequencies. In the high-frequency mode, VD and DD motoneurons have different inactive phases; in the low-frequency mode, VD and DD motoneurons showed similar wide inactive phases.

**Computational models tested three hypotheses for the role of inhibition in fast locomotion.**

Based on the experimental results, we suggest five hypotheses to explain the role of inhibition in sustaining high-frequency locomotion. First, it has long been suggested that cross-inhibition of the opposing body wall muscles increases the dorsoventral difference in muscle activation (McIntire 1993a, Bryden and Cohen 2008). Second, disinhibition of the innervated body wall muscles increases muscle activation, particularly during the rising phase. Third, inhibitory reset of VA and VB by the VD motoneurons allows higher locomotion frequency through phasic inhibition of ventral motoneurons (consistent with Boyle *et al*., 2012). Fourth, VD disinhibition of the VA and VB ventral cholinergic motoneurons amplifies, particularly during their rising phase. Fifth, reciprocal inhibition between VD and DD motoneurons stabilizes dorsoventral alternation.

From the experimental results, we found that *vab-7* mutants (in which DB neurons differentiate as VA) and *unc-4* mutants (in which DA and VA differentiate as DB and VB) were not different from the wild type in their shrinking response to harsh head and tail touch, respectively. This suggests that the mechanism for the shrinking response is not caused by coactivation of forward and backward premotor interneurons (AVA and AVB); instead, it appears localized within the motor circuit. Furthermore, shrinking appears qualitatively similar in the forward and backward motor circuits. We therefore focused our computational models on forward locomotion. Our model results can be reproduced for backward locomotion by changing the direction of the propagating wave under feedforward control or by changing the direction of the proprioceptive field under feedback control (Denham *et al.* 2018). Our model results are only applied within the scope of the function of inhibition, and we do not assume that forward and backward circuits are driven by the same mechanism nor do we model the transitions between forward and backward locomotion.

There are two prevalent hypotheses to explain the undulatory body bends in *C. elegans*: the proprioception (feedback-driven) hypothesis and the endogenous oscillator (feedforward-driven or central pattern generator) hypothesis. Proprioception transduces body curvature to adjacent body segments, so that rhythmic movement propagates along the body; endogenous oscillators (CPG circuits) generate rhythmic movement at the head or tail of the animal, or along the body

(Gjorgjieva *et al.*, 2014). Although proprioception and endogenous oscillators have been evidenced in *C. elegans*, their relative contributions during locomotion remain to be determined (Fouad *et al.*, 2018, Xu *et al.*, 2018, Gao *et al.*, 2018). Previous models (Denham *et al*., 2018; Izquierdo and Beer, 2018) have investigated these regimes separately in order to parse their qualitative differences.

The models we used in this study are based on evidence for proprioceptive mechanisms (Wen *et al.*, 2012) and for endogenous oscillators that could provide feedforward motor control (Gao *et al.*, 2018). Using a proprioceptive model, we tested cross-inhibition, disinhibition, and inhibitory reset. Using a CPG-driven model, we tested muscle cross-inhibition and muscle disinhibition. The role of GABAergic motoneurons in rhythm generation in the *C. elegans* nerve cord remains uncharacterized and is not addressed in our models. In particular, more detailed neural models would be required to test VD disinhibition of VA and VB motoneurons and reciprocal inhibition between VD and DD motoneurons. In addition, a consequence of modeling purely feedforward, CPG-driven motor activity is the absence of a mechanism for the modulation of frequency, e.g., in response to changes in environmental viscosity. For both models, we simulated locomotion in two environments (agar-like and liquid-like) but did not directly manipulate undulation frequency within a given environment. We simulated forward locomotion in agar-like and liquid-like environments under proprioceptive and CPG control. Then, we compared simulations of wild-type animals with simulations that incorporate perturbations of the neuromuscular input due to the omission of cross-inhibition, disinhibition, or both (Fig. 8c).

Under proprioceptive control, we find that all three perturbations induced a substantial decrease in undulation frequency. Simulated mutants lacking cross-inhibition of the opposing muscles showed the largest reduction (25% and 28% of simulated wild-type frequency in agar-like and liquid-like environments, respectively, in response to a 20% change in muscle input) followed by simulated mutants lacking disinhibitory rebound in the innervated muscle (22% and 20% of wild-type frequency in agar-like and liquid-like environments, respectively, in response to a 20% change in muscle timescale). Applying both manipulations simultaneously decreased undulation frequency of the wild type even further (by 34% and 42% in agar-like and liquid-like environments, respectively). Intuitively, for proprioceptive control, continuous activation within the antagonistic muscle during bending causes stiffness of muscles, slowing down bending, and in turn delaying the state switch of the adjacent motoneurons (i.e., the propagation of the undulatory wave). The same simulations also showed a decrease in overall locomotion speed, which was proportional to the frequency decrease in liquid, but disproportionately small in agar. In contrast, in our model of CPG control, muscle inhibition had no effect on the undulation frequency. We also found that removing cross-inhibition of model muscles results in reduced speed, whereas removing muscle disinhibition resulted in increased locomotion speeds, indicating that the propagation of smooth sinusoidal, rather than square, muscle activation wave is mechanically more efficient (Lighthill, 1960). Together, these results suggest that the observed frequency–speed dependence is a signature of proprioceptively driven neural control. Our model further suggests that inhibition of GABAergic motoneurons influences undulation frequency primarily at the neuromuscular junctions. We note that additional frequency modulation mechanisms, which lie outside the scope of our model, cannot be ruled under combined CPG and proprioceptive control.

We next tested the inhibitory resetting of VB by VD motoneurons. A neuromechanical model by Boyle *et al.* (2012) suggests that as a consequence of bistability of the A- and B-type motoneurons (Liu *et al.* 2014), ventral and dorsal motoneurons may simultaneously occupy the same state, effectively pausing locomotion in a manner that is reminiscent of the *shrinker*

phenotype. To resume healthy locomotion, Boyle *et al*. (2012) proposed that inhibition from VD to VB motoneurons acts as a neural reset mechanism, switching VB off in order to facilitate a dorsal bend. Simulations of Boyle *et al*.'s model show that this neural reset has little effect on slow locomotion (in an agar-like environment) but is required for coordinated undulations during fast locomotion (in a liquid-like environment). This result inspired our third hypothesis and the reimplementation of this mechanism in the current model (see Methods). We simulated nematodes lacking neural inhibition from VD to VB motoneurons in our proprioceptive model. The simulated mutant did not show any significant change in frequency in an agar-like environment (Fig. 8cd). However, when simulated in a liquid-like environment, these simulated mutants became severely uncoordinated and failed to make progress, consistent with Boyle *et al.* (2012). This result indicates a requirement for a neural inhibitory reset mechanism to sustain coordinated fast undulations, at least in the absence of additional backup mechanisms (such as CPG control).

To summarize, our model results suggest that under proprioceptively driven locomotion, muscle cross-inhibition enhances locomotion frequency and speed. The associated frequency–speed dependence is consistent with our experimental observations. In this model, cross-inhibition and disinhibition of the body-wall muscles supports high-frequency undulatory locomotion, whereas the neural inhibition within the motor circuit can stabilize high-frequency undulations.

## Discussion

We investigated the role of inhibition in locomotion by analyzing the behavior of wild-type and mutant animals, recording neuronal and muscular activity in undulating intact animals, and by testing possible mechanisms with computational models. Both wild type and GABA transmission mutants responded to harsh touch to the head or tail by shrinking, suggesting that dorsoventral coactivation is produced by the unimpaired nervous system. Impairment of GABA transmission genetically or optogenetically induced lower undulation frequency and translocation speed during crawling and swimming in both directions. GABAergic motoneurons' activity patterns were different during undulation at low and high frequencies. During low undulation frequency, VD and DD showed a similar activity pattern, while during high undulation frequency, their activity alternated. We suggested five hypotheses for inhibitory mechanisms that support rapid undulation and tested three of them computationally. Our modeling results suggested that cross-inhibition and disinhibition of the body-wall muscles support rapid undulation. Finally, we suggest that the unimpaired locomotion circuit operates at two distinct modes to produce an undulatory motor program at low and high frequencies.

### Shrinking occurs in wild type and GABA transmission mutants

The shrinking response, presumably from coactivation of the dorsoventral muscle, has been described in GABA transmission mutants (McIntire *et al*., 1993a; McIntire *et al*., 1993b) and following laser ablation of GABAergic motoneurons (Yanik *et al*., 2004). Here, we show that shrinking commonly occurs in wild type in response to harsh touch stimuli to the head or tail. The shrinking response does not require the simultaneous contribution of cholinergic motoneurons associated with the forward and backward directions. Neurodevelopmental mutant animals (namely, *vab-7* and *unc-4*) with impaired A- or B-type cholinergic motoneurons, respectively, show a shrinking response after the harsh touch stimulation that induces their normal undulatory locomotion (e.g., harsh head touch to *vab-7* induces wild-type-like sinusoidal backward

undulation). These results suggest that shrinking is not associated with backward locomotion or with a change in direction, but rather with the switch from slow to fast locomotion and that shrinking is part of the motor program produced by the unimpaired nervous system.

The shrinking phenotype was first described in mutants and not discovered in wild-type animals (McIntire *et al*., 1993a; McIntire *et al*., 1993b), probably because the latter resolves the coactivation and swiftly moves away from noxious stimuli. Video microscopy and frame-by-frame inspection are therefore required to capture the brief body shrinkage of wild-type animals. Morphological measurement of the change in body length before and after harsh touch stimulation revealed that every animal, either wild type or the GABA transmission knockouts, shrank. It is the longer lasting shrinkage and lower translocation speed of GABA transmission mutants, which makes the observation of the shrinking phenotype easier with the naked eye.

**The distinct phenotype of the GABA transmission mutants is slow swimming**

GABA transmission mutants, colloquially named '*shrinkers'*, such as *unc-46* and *unc-47* mutant strains defective in GABA vesicular transporter and *unc-49* mutant strain defective in anionic $GABA_A$ receptors, have been described as defective in backward locomotion because they fail to produce wild-type-like swift reversal following a harsh touch on the head (McIntire *et al*., 1993a; McIntire *et al*., 1993b; Schuske *et al*., 2004). A similar phenotype was described in animals after laser ablation (Yanik *et al*., 2004). However, we found that the shrinking phenotype is not related to the target of noxious stimuli or the direction of locomotion, as GABA transmission mutants shrink in response to harsh touch to the tail as well as the head. Moreover, wild-type animals exhibit a shrinking phenotype, although smaller in magnitude and quicker to resolve. When suspended in liquid, GABA transmission mutants are uncoordinated and swim slowly with lower undulation frequency and translocation speed compared to those of the wild type. They exhibit a similar but less prominent phenotype when crawling on agar plates. Hence, slow and uncoordinated swimming, rather than shrinking, is a distinct phenotype of GABA transmission mutants.

**GABA transmission is necessary for fast dorsoventral alternation**

During free crawling or swimming in either direction, an acute or chronic absence of GABA transmission leads to lower undulation frequency and translocation speed. The effect is more severe during swimming, which is typically performed at higher undulation frequency. Even following noxious touch stimuli that induce a rapid escape response in the wild type, GABA transmission mutants do not increase their undulation frequency and translocation speed and are slower than those of the wild type. These results deem GABA transmission necessary for fast locomotion.

The undulation frequency dictates translocation speed during sinusoidal crawling and swimming behaviors in wild-type and mutant animals. Correlations between undulation frequency and translocation speed were always positive. The slope of the linear regression was always steeper for the wild type, suggesting a more efficient translation of undulation frequency to translocation speed. This suggests a subtle contribution of inhibition to the motor program of slow locomotion because the data for locomotion of mutant animals is for slower translocation speed. Shape related parameters such as amplitude and wavelength are weakly correlated to instantaneous translocation speed, although they may contribute to fast locomotion.

## GABAergic motoneurons exhibit dorsoventral alternating inactive phases that match the activation of their postsynaptic body-wall muscles only during high-frequency undulation

Morphologically, GABAergic motoneurons synapse to the muscle arms of body-wall muscles (White *et al*., 1976, 1986), and their inhibitory effect on body-wall muscles was confirmed by laser ablation, muscle electrophysiology during bath application of GABA, and activation GABAergic motoneurons optogenetically (McIntire *et al*., 1993b; Bamber *et al*., 2005; Gao and Zhen, 2011; Inoue *et al*., 2015). The neuronal activity of GABAergic motoneurons has not been reported and was presumed to be similar to that of its antagonistic muscle, as both are activated by the same excitatory motoneurons. However, when we recorded the changes in calcium levels in GABAergic motoneurons during undulations, we found that they exhibited a baseline level of calcium signal interspaced by phases of lower signal and that the pattern of activity was frequency dependent. In high-frequency undulation, when calcium signal level in ventral body-wall muscle cells increased during contraction around 270° of the locomotion cycle, the calcium signal in VD motoneurons decreased; and when the calcium signal level in dorsal body-wall muscle cells increased during contraction around 90°, the calcium signal in DD motoneurons decreased (Fig. 7). These are possibly inactivity windows that allow postsynaptic muscles to escape from inhibition and be activated more sharply, or they could amplify muscle activity through disinhibition. In contrast, during low-frequency undulation, VD and DD exhibit similar patterns of calcium signal changes with a wide trough from 90° to 270°, which includes portions of ventral and dorsal bending regions. Hence, our calcium imaging of GABAergic motoneurons further supports their involvement in high-frequency undulations as their activity patterns are different for low and high undulation frequencies.

## Other possible inhibitory roles of GABAergic motoneurons in high-frequency undulation

GABAergic motoneurons might play several inhibitory roles during high-frequency undulation. We tested three hypotheses for the neuronal mechanisms that underlie these roles using proprioceptive mechanisms control and feedforward motor control models: 1) Cross-inhibition, in which when the body wall muscle is activated, the coactivated GABAergic motoneurons inhibit the opposing body wall muscle; 2) disinhibition of the innervated body wall muscles, in which the release from inhibition enhances muscle activation, particularly during its rising phase; 3) inhibitory reset of VA and VB, in which VD input terminates the locomotion cycle early and allows higher locomotion frequency (Boyle *et al*., 2012; Cohen and Sanders, 2014; Cohen and Denham, 2019). Our model results suggest that cross-inhibition and disinhibition of the body-wall muscles supports high-frequency undulatory locomotion, whereas the neural inhibition within the motor circuit stabilizes such high-frequency undulations. Besides the aforementioned roles of inhibition, there are other possible roles that we did not test because of experimental or computational model limitations. First, VD disinhibition of VA and VB, in which the activation of ventral cholinergic motoneurons is amplified, particularly during their rising phase. Second, reciprocal or nonreciprocal inhibition between DD and VD motoneurons, which might reinforce the antiphasic activity of GABAergic motoneurons during rapid locomotion. These inhibition or disinhibition are not exclusive in sustaining the fast dorsoventral body-wall muscle alternation. Cross-inhibition and disinhibition of muscles fulfill the activation–relaxation alternation of dorsoventral muscles, and neural inhibition helps to stabilize the motor circuit.

## Two modes of locomotion

We have demonstrated that the inhibitory motoneurons of the locomotion circuit are necessary only for rapid undulations and that their activity patterns are different for rapid and slow undulations. The frequency-dependent activity pattern of inhibitory motoneurons, the brief shrinking behavior when initiating an escape response, and the absence of rapid undulations when inhibition is inactive suggests a role for inhibition in the unimpaired nervous system. In addition, the distributions of frequency and translocation speed during crawling in both directions in the wild type are bimodal. Together, these results suggest that the locomotion circuit produces an undulatory motor program by two distinct modes of operation: low-frequency undulations that do not require inhibition and high-frequency undulations that require inhibition and in which GABAergic motoneurons exhibit an alternating activity pattern.

## References


Ahringer J (2006) Reverse genetics. In: *WormBook*, ed. The *C. elegans* Research Community, WormBook.

Alon U (2007). Network motifs: theory and experimental approaches. Nature Reviews Genetics, 8(6), 450-461.

Altun ZF, Hall DH (2009) Muscle system, somatic muscle. In WormAtlas.

Bamber BA, Richmond JE, Otto JF, Jorgensen EM (2005) The composition of the GABA receptor at the *Caenorhabditis elegans* neuromuscular junction. Br J Pharmacol 144:502-509.

Berri S, Boyle JH, Tassieri M, Hope IA, Cohen N (2009) Forward locomotion of the nematode *C. elegans* is achieved through modulation of a single gait. HFSP J 3:186-193.

Boyle JH, Berri S, Cohen N (2012) Gait Modulation in *C. elegans*: An Integrated Neuromechanical Model. Front Comput Neurosci 6:10.

Brenner S (1974) The genetics of *Caenorhabditis elegans*. Genetics 77:71-94.

Bryden J, Cohen N (2008). Neural control of *Caenorhabditis elegans* forward locomotion: the role of sensory feedback. Biological cybernetics, 98(4), 339-351.

Butler VJ, Branicky R, Yemini E, Liewald JF, Gottschalk A, Kerr RA, Chklovskii DB, Schafer WR (2015) A consistent muscle activation strategy underlies crawling and swimming in *Caenorhabditis elegans*. J R Soc Interface 12:20140963.

Chen BL, Hall DH, Chklovskii DB (2006) Wiring optimization can relate neuronal structure and function. Proc Natl Acad Sci 103:4723-4728.

Cohen N, Denham JE (2019) Whole animal modeling: piecing together nematode locomotion. Curr Opin Syst Biol 13:150-160.

Cohen N, Ranner T (2017) A new computational method for a model of *C. elegans* biomechanics: Insights into elasticity and locomotion performance. arXiv:1703.04988.

Cohen N, Sanders T (2014) Nematode locomotion: dissecting the neuronal–environmental loop. Curr Opin Neurobiol 25:99–106.

Corsi AK, Wightman B, Chalfie M (2015) A Transparent window into biology: A primer on *Caenorhabditis elegans*. In: *WormBook*, ed. The *C. elegans* Research Community, WormBook.

Denham JE, Ranner T, Cohen N (2018) Signatures of proprioceptive control in *Caenorhabditis elegans* locomotion. Philos Trans R Soc Lond B Biol Sci 373.

Donnelly JL, Clark CM, Leifer AM, Pirri JK, Haburcak M, Francis MM, Samuel AD, Alkema MJ (2013) Monoaminergic orchestration of motor programs in a complex *C. elegans* behavior. PLoS Biol 11:e1001529.

Emmons SW (2015) The beginning of connectomics: a commentary on White *et al*. (1986) 'The structure of the nervous system of the nematode *Caenorhabditis elegans'*. Philos Trans R Soc Lond B Biol Sci 370.

Esmaeili B, Ross JM, Neades C, Miller DM, 3rd, Ahringer J (2002) The *C. elegans* even-skipped homologue, vab-7, specifies DB motoneurone identity and axon trajectory. Development 129:853-862.

Fouad AD, Teng S, Mark JR, Liu A, Alvarez-Illera P, Ji H, Du A, Bhirgoo PD, Cornblath E, Guan SA, Fang-Yen C (2018). Distributed rhythm generators underlie *Caenorhabditis elegans* forward locomotion. Elife, 7, e29913.

Gao S, Zhen M (2011) Action potentials drive body wall muscle contractions in *Caenorhabditis elegans*. Proc Natl Acad Sci 108:2557-2562.

Gao S, Guan SA, Fouad AD, Meng J, Kawano T, Huang YC, Li Y, Alcaire S, Hung W, Lu Y, Qi YB, Jin Y, Alkema M, Fang-Yen C, Zhen M (2018) Excitatory motor neurons are local oscillators for backward locomotion. eLife 7.

Gershenson C, Helbing D (2015). When slower is faster. Complexity, 21(2), 9-15.

Gjorgjieva J, Biron D, Haspel G (2014) Neurobiology of *Caenorhabditis elegans* Locomotion: Where Do We Stand? Bioscience 64:476-486.

Haspel G, O'Donovan MJ (2011) A perimotor framework reveals functional segmentation in the motoneuronal network controlling locomotion in *Caenorhabditis elegans*. J Neurosci 31:14611-14623.

Haspel G, O'Donovan MJ, Hart AC (2010) Motoneurons dedicated to either forward or backward locomotion in the nematode *Caenorhabditis elegans*. J Neurosci 30:11151-11156.

Inoue M, Takeuchi A, Horigane S, Ohkura M, Gengyo-Ando K, Fujii H, Kamijo S, Takemoto-Kimura S, Kano M, Nakai J, Kitamura K, Bito H (2015) Rational design of a high-affinity, fast, red calcium indicator R-CaMP2. Nat Methods 12:64-70.

Izquierdo EJ, Beer RD (2018) From head to tail: a neuromechanical model of forward locomotion in *Caenorhabditis elegans*. Philos Trans R Soc Lond B Biol Sci 373.

Javer A, Currie M, Lee CW, Hokanson J, Li K, Martineau CN, Yemini E, Grundy LJ, Li C, Ch'ng Q, Schafer WR, Nollen EAA, Kerr R, Brown AEX (2018) An open-source platform for analyzing and sharing worm-behavior data. Nat Methods 15:645-646.

Karbowski J, Cronin CJ, Seah A, Mendel JE, Cleary D, Sternberg PW (2006) Conservation rules, their breakdown, and optimality in *Caenorhabditis* sinusoidal locomotion. J Theor Biol 242:652-669.

Kiehn O (2011) Development and functional organization of spinal locomotor circuits. Current opinion in neurobiology 21:100-109.

Kiehn O (2016) Decoding the organization of spinal circuits that control locomotion. Nat Rev Neurosci 17:224-238.

Lighthill M (1960) Note on the swimming of slender fish. J Fluid Mech , 9:305-317.

Liu P, Chen B, Wang Z-W (2014) SLO-2 potassium channel is an important regulator of neurotransmitter release in *Caenorhabditis elegans.* Nat Commun, 5:5155.

Lockery SR, Lawton KJ, Doll JC, Faumont S, Coulthard SM, Thiele TR, Chronis N, McCormick KE, Goodman MB, Pruitt BL (2008) Artificial dirt: microfluidic substrates for nematode neurobiology and behavior. J Neurophysiol 99:3136-3143.

Mattis J, Tye KM, Ferenczi EA, Ramakrishnan C, O'Shea DJ, Prakash R, Gunaydin LA, Hyun M, Fenno LE, Gradinaru V, Yizhar O, Deisseroth K (2011) Principles for applying optogenetic tools derived from direct comparative analysis of microbial opsins. Nat Methods 9:159-172.

McIntire SL, Jorgensen E, Horvitz HR (1993a) Genes required for GABA function in *Caenorhabditis elegans*. Nature 364:334-337.

McIntire SL, Jorgensen E, Kaplan J, Horvitz HR (1993b) The GABAergic nervous system of *Caenorhabditis elegans*. Nature 364:337-341.

Miller DM, Shen MM, Shamu CE, Burglin TR, Ruvkun G, Dubois ML, Ghee M, Wilson L (1992) *C. elegans* unc-4 gene encodes a homeodomain protein that determines the pattern of synaptic input to specific motor neurons. Nature 355:841-845.

Miller DM, 3rd, Niemeyer CJ (1995) Expression of the unc-4 homeoprotein in *Caenorhabditis elegans* motor neurons specifies presynaptic input. Development 121:2877-2886.

Nagel G, Brauner M, Liewald JF, Adeishvili N, Bamberg E, Gottschalk A (2005) Light activation of channelrhodopsin-2 in excitable cells of *Caenorhabditis elegans* triggers rapid behavioral responses. Curr Biol : CB 15:2279-2284.

Okazaki A, Sudo Y, Takagi S (2012) Optical silencing of *C. elegans* cells with arch proton pump. PloS One 7: e35370.

Petrash HA, Philbrook A, Haburcak M, Barbagallo B, Francis MM (2013) ACR-12 ionotropic acetylcholine receptor complexes regulate inhibitory motor neuron activity in *Caenorhabditis elegans*. J Neurosci 33:5524-5532.

Pierce-Shimomura JT, Chen BL, Mun JJ, Ho R, Sarkis R, McIntire SL (2008) Genetic analysis of crawling and swimming locomotory patterns in *C. elegans*. Proc Natl Acad Sci 105:20982-20987.

Ranner T (2020). A stable finite element method for low inertia undulatory locomotion in three dimensions. Applied Numerical Mathematics 156:422-445.

Roberts A, Li WC, Soffe SR (2008) Roles for inhibition: studies on networks controlling swimming in young frog tadpoles. J Comp Physiol A Neuroethol Sens Neural Behav Physiol 194:185-193.

Schuske K, Beg AA, Jorgensen EM (2004) The GABA nervous system in *C. elegans*. Trends Neurosci 27:407-414.

Stephens GJ, Johnson-Kerner B, Bialek W, Ryu WS (2008) Dimensionality and dynamics in the behavior of *C. elegans*. PLoS Comput Biol 4: e1000028.

Wen Q, Po MD, Hulme E, Chen S, Liu X, Kwok SW, Gershow M, Leifer AM, Butler V, Fang-Yen C, Kawano T, Schafer WR, Whitesides G, Wyart M, Chklovskii DB, Zhen M, Samuel AD (2012) Proprioceptive coupling within motor neurons drives *C. elegans* forward locomotion. Neuron 76:750-761.

White JG, Southgate E, Thomson JN, Brenner S (1976) The structure of the ventral nerve cord of *Caenorhabditis elegans*. Philos Trans R Soc Lond B Biol Sci 275:327-348.

White JG, Southgate E, Thomson JN, Brenner S (1986) The structure of the nervous system of the nematode *Caenorhabditis elegans*. Philos Trans R Soc Lond B Biol Sci 314:1-340.

Yanik MF, Cinar H, Cinar HN, Chisholm AD, Jin Y, Ben-Yakar A (2004) Neurosurgery: functional regeneration after laser axotomy. Nature 432:822.

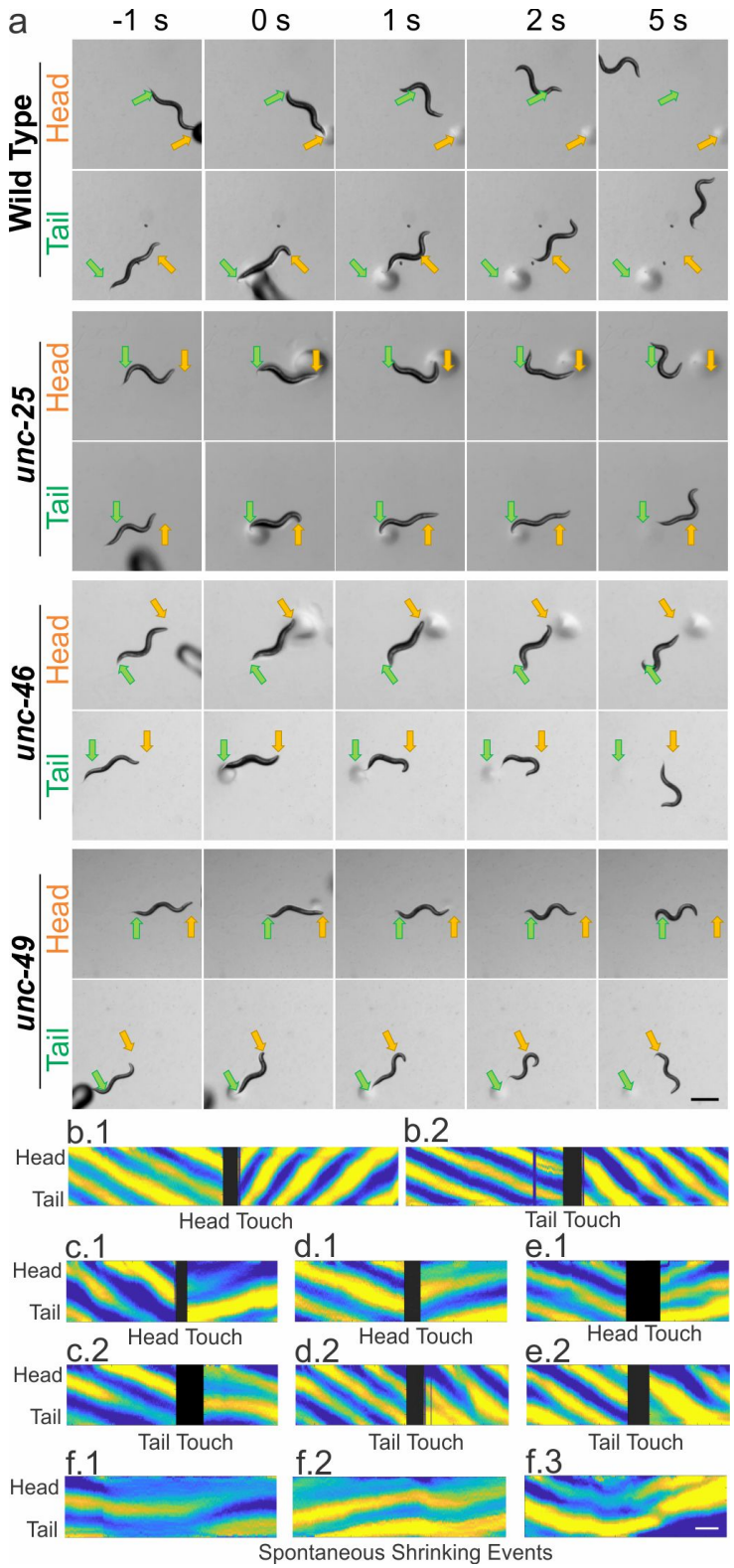


**Figure 1.** Wild type and GABA transmission knockouts shrank after harsh touch to the head or tail, while only wild type escaped rapidly. (a) While moving forward, animals were touched by a blunt glass probe as a harsh stimulation to the head (yellow arrow) or tail (green arrow). Wild type animals briefly shrank immediately after stimulation (0 s compare to -1 s before stimulation) and rapidly moved away from the stimuli, while GABA transmission knockouts shrank for a longer time and moved away slowly. Note that by 5 s all animals had moved away from the stimuli. Scale bar = 0.5 mm. Dark and circular shadows were the glass probe and the marks it left on agar. After harsh stimulation, wild type animals (b) increased undulation frequency to escape backwards (b.1) or forwards (b.2), while the three GABA transmission mutants – *unc-25* (c), *unc-46* (d) and *unc-49* (e) – moved away from the stimulus but decreased undulation frequency. Moreover, there was a period in which the body posture of these mutants did not change after the stimulation (c-e). The mutants, *unc-25* (f.1), *unc-46* (f.2) and *unc-49* (f.3), occasionally shrank without stimulation. Yellow and blue shaded area in b-f represent dorsoventral curvature (y axis is the length of animal from the head on the top to the tail), along time (x axis, scale bar is 1 s); black blocks, indicating the harsh touch stimulation, were caused by probe.

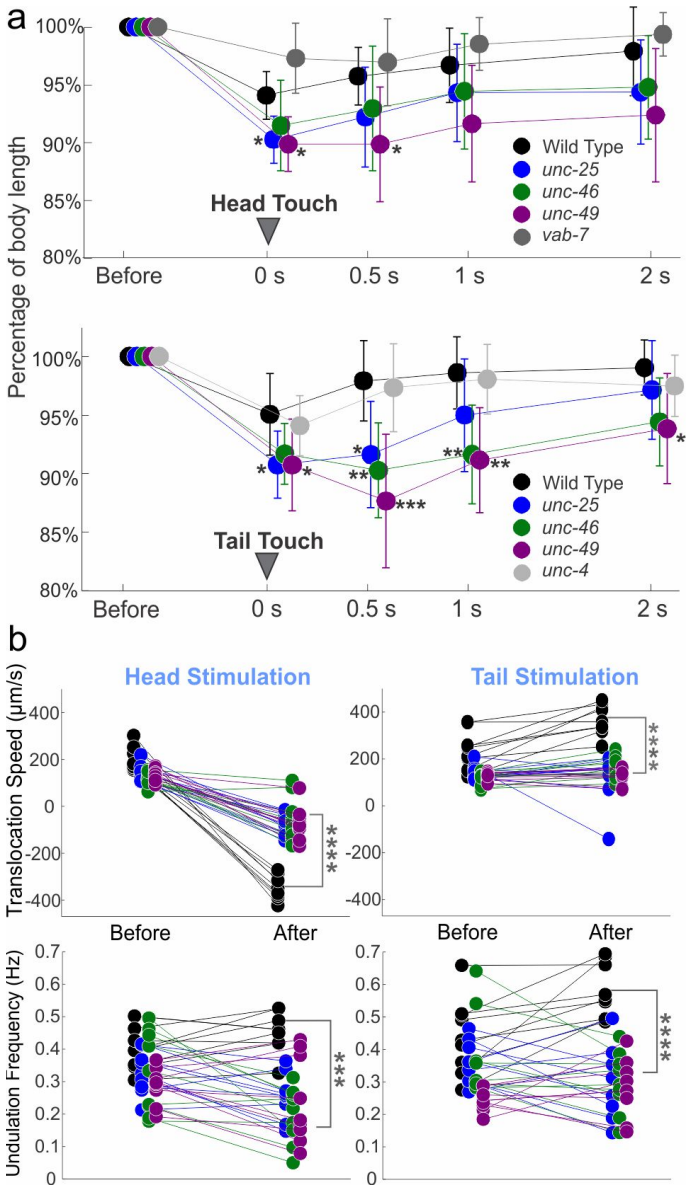
a
Percentage of body length
100%
95%
90%
85%
80%
Head Touch
Before
0 s
0.5 s
1 s
2 s
Wild Type
unc-25
unc-46
unc-49
vab-7
Tail Touch
unc-4
b
Translocation Speed (μm/s)
Head Stimulation
Tail Stimulation
400
200
0
-200
-400
Before
After
Undulation Frequency (Hz)
0.7
0.6
0.5
0.4
0.3
0.2
0.1
0

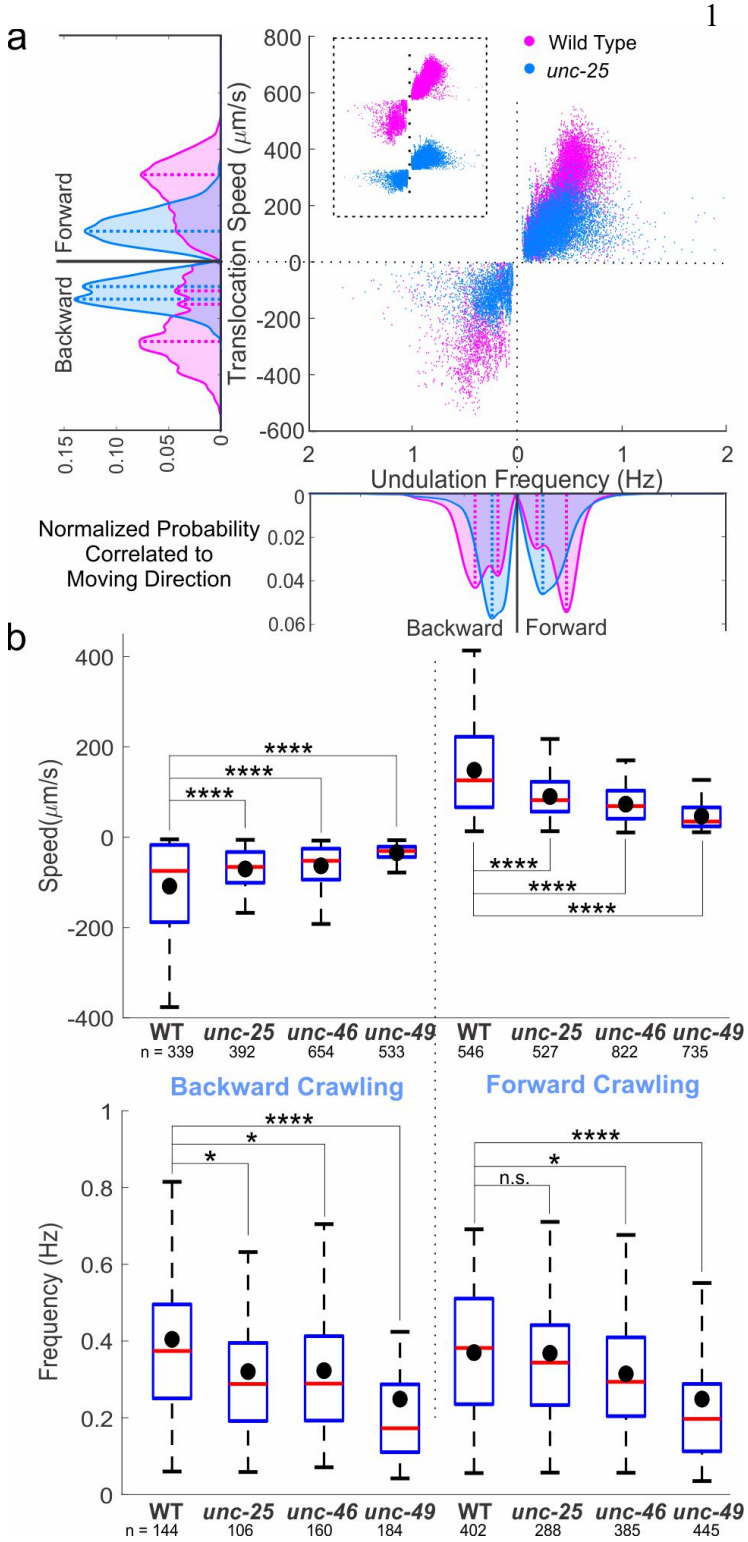


**Figure 3.** GABA transmission mutants crawled slower than wild type. (a) *unc-25* knockout animals crawled on agar surface with lower translocation speed and undulation frequency than wild type. Negative translocation speed and undulation frequency left of 0 represent backward locomotion. Area plots are probability occurrence within each direction either forward or backward. The dashed lines indicate the main peaks in the area plots. The area plots were generated from histograms. The bin size of the translation speed histogram was 20 um/s, and that of the undulation frequency histogram was 0.02 Hz. (b) Translocation speeds of all the GABA transmission knockouts were significantly lower than that of wild type (WT) during forward and backward crawling. The undulation frequencies of GABA transmission knockouts were significantly lower than that of wild type, except for that of *unc-25* during forward crawling. Blue boxes range the first to third quartiles of each dataset, red lines are medians, black dots are mean values, the bottom and top black whisker are the minimum and the maximum, respectively, excluding outliers (beyond 1.5-fold interquartile range from middle 50% data). ANOVA with Tukey pairwise comparison to wild type, n.s. $p>0.05$, * $p<0.05$, *** $p<0.001$, **** $p<0.0001$. See table 3-1 for details.

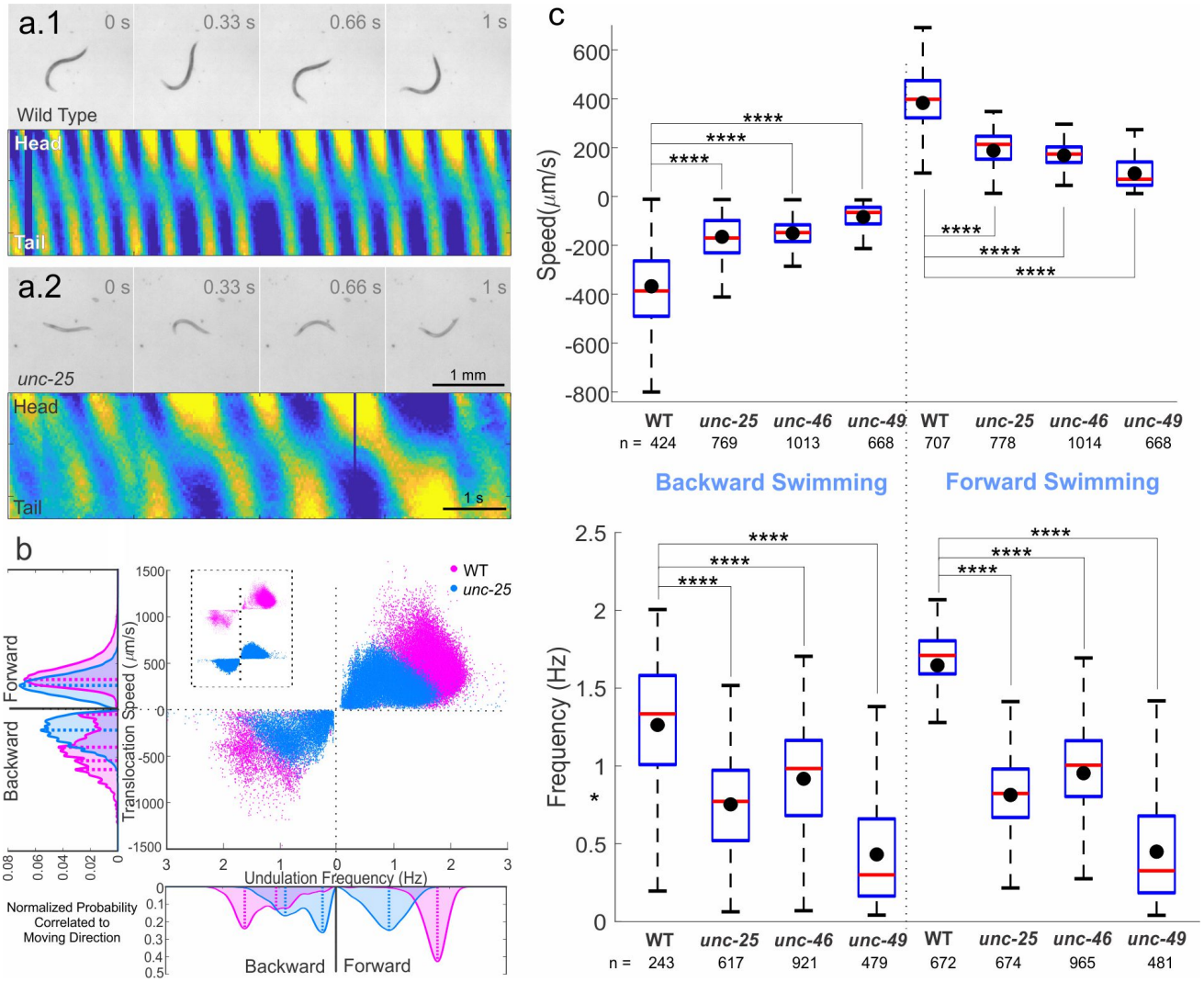


**Figure 4.** GABA transmission knockouts swam slower than wild type. Compared to wild type (a.1), *unc-25* knockout (a.2) swam in liquid with lower undulation frequency and translocation speed, as well as smaller undulation amplitude and wavelength. Video frames are 0.33 s apart, scale bars are 1 mm; and kymograms are color coded as in Figure 2, scale bars are 1 s. (b) Wild type swam faster with higher translocation speed and undulation frequency, compared to *unc-25* knockout. Area plots are probability occurrence within each direction, forward or backward. The dashed lines indicate the main peaks in the area plots. The area plots were generated from histograms. The bin size of the translation speed histogram was 24 um/s, and that of the undulation frequency histogram was 0.05 Hz. (c) Translocation speeds and undulation frequencies of all the GABA transmission knockouts were significantly lower than those of wild type (WT) during forward and backward swimming. Box plots as in Fig. 4. ANOVA with Tukey pairwise comparison to wild type, **** $p<0.0001$. See Table 4-1 for details.

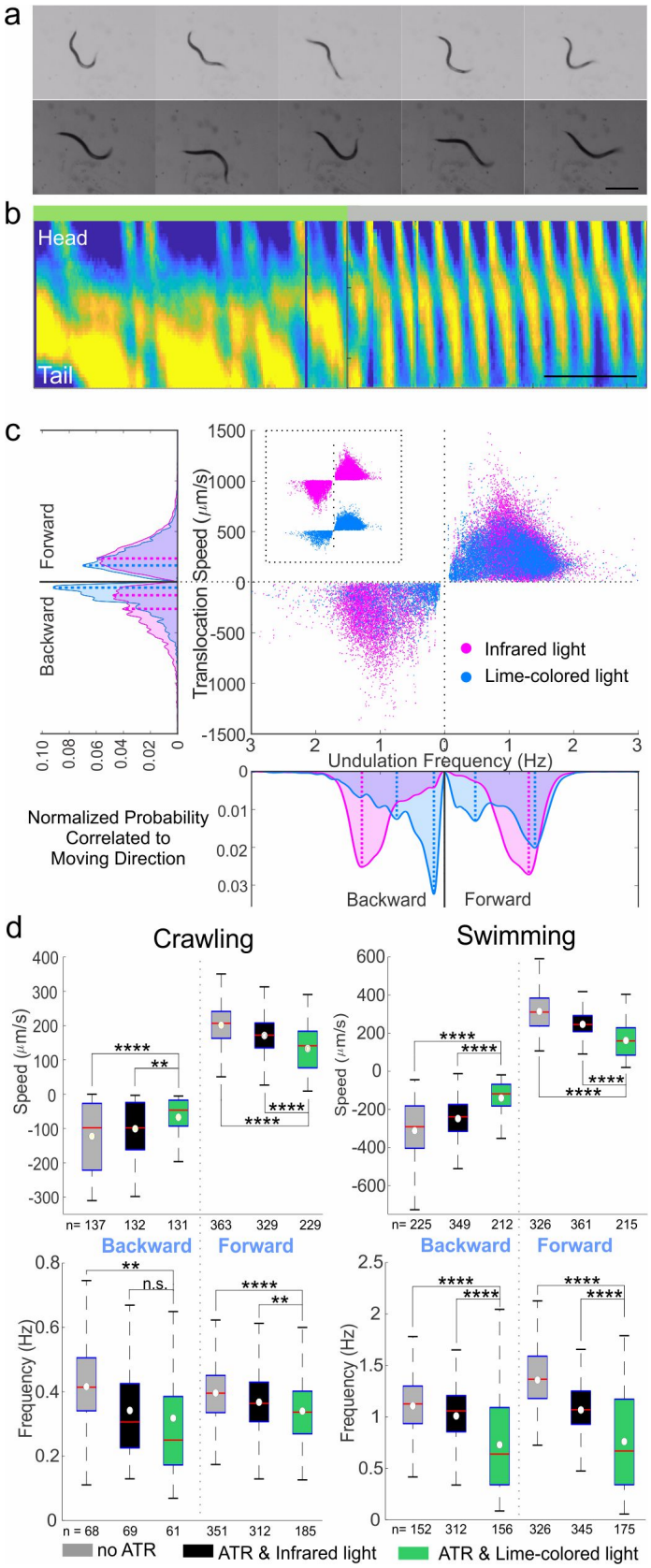


**Figure 5.** Acute inactivation in GABAergic motoneurons induced slow locomotion during swimming and crawling. (ab) When GABAergic motoneurons were inactivated optogenetically (top framed of a, and green line on top of b) while swimming in liquid, undulations were slower and more uncoordinated. When the optogenetic inhibition was withdrawn (bottom frames of a, and grey line in b), the animal regained coordinated undulatory swimming and its undulation frequency doubled from 0.5 to 1 Hz. Frame rate in a is 3 fps. (c) The optogenetic strain fed with ATR swam slower when optogenetically inactivated (by lime-colored light) compared to the same animals under infrared light. The area plots were generated from histograms. The bin size of the translation speed histogram was 24 um/s, and that of the undulation frequency histogram was 0.05 Hz. (d) When GABAergic motoneurons were acutely inhibited (green boxes, ATR and lime-colored light), animals crawled and swam at significantly lower translocation speed and undulation frequency compared to two negative controls -- the same animal under infrared light (black boxes) and the same strain not fed ATR (grey boxes), except for backward-crawling undulation frequency of the animal under lime-colored light and infrared light were not statistically different. Boxplot design similar to Figures 4-5. ANOVA with Tukey pairwise comparison to the animal fed with ATR and under lime-colored light, n.s. $p>0.05$, ** $p<0.1$, **** $p<0.0001$. See Table 5-1 for details

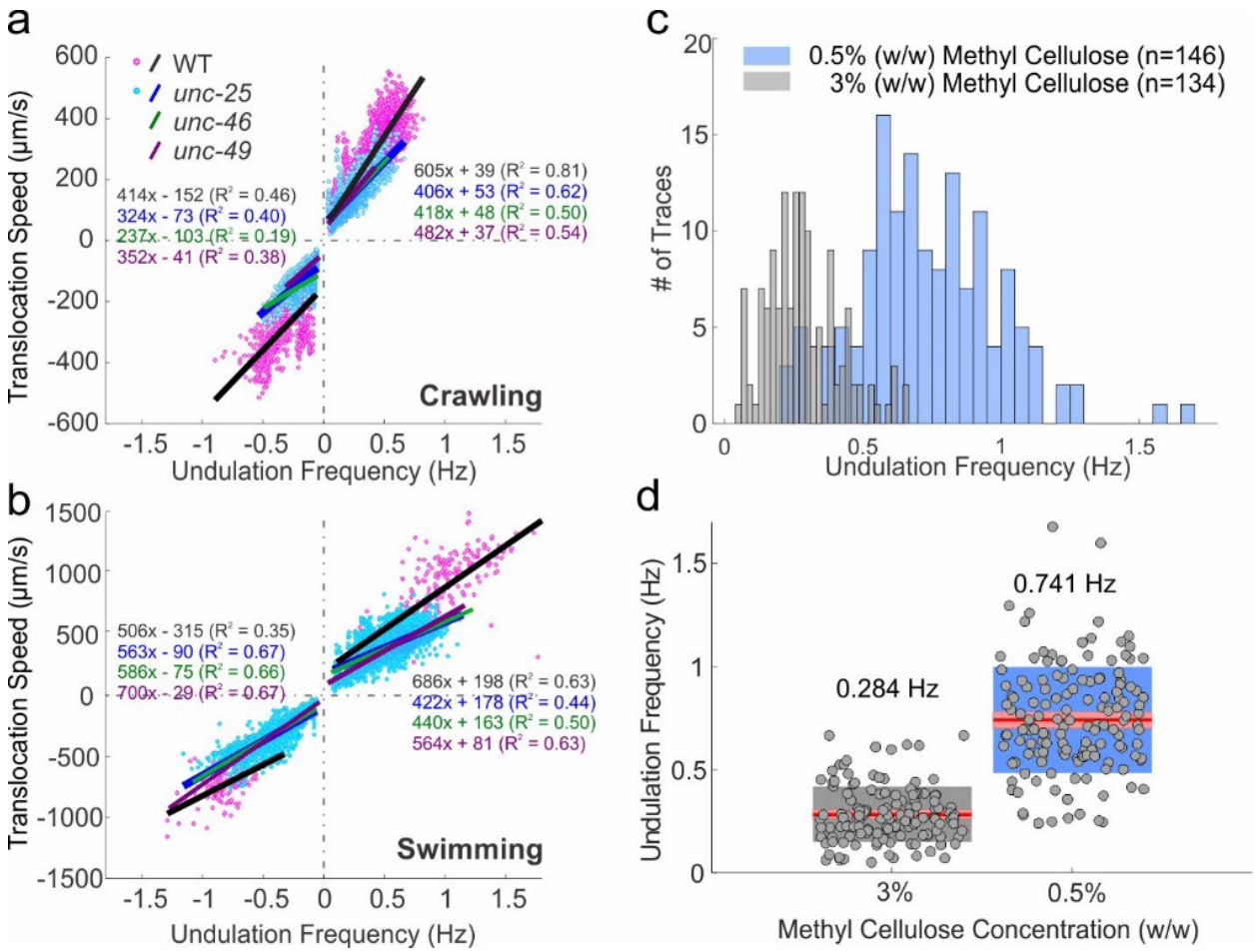


**Figure 6.** During sinusoidal undulation, the undulation frequency correlates to translocation speed; different relevant undulations frequencies were induced by setting ambient viscosity in the microfluidic waveform channels. (ab) Undulation frequency was positively correlated with translocation speed during crawling and swimming. Wild type (magenta dots) and *unc-25* (cyan dots) data were selected from time in which animals performed sinusoidal locomotion. Fitted linear regression lines of wild type (black), *unc-25* (blue), *unc-46* (green) and *unc-49* (purple) strains, coefficients of determination ($R^2$) and equations are labeled in with the same colors. (c) In waveform microfluidic device, animals can undulate in predetermined channels designed to restrict their path. When the ambient viscosity was high (3% methyl cellulose solution) wild type undulated in lower undulation frequencies than in less viscous environment, (0.5% methyl cellulose solution). Frequency was measured by the movement of neurons and muscle during calcium imaging and sample size (n) is the number of cells analyzed. (d) Same data as c. The average undulation frequency in 3% methyl cellulose solution was 0.28±0.14, and that in 0.5% solution was 0.74±0.26 Hz. Red lines are mean values, pink boxes are 95% confidence intervals for the mean, gray and blue boxes are standard deviation, and gray dots are individual data points.

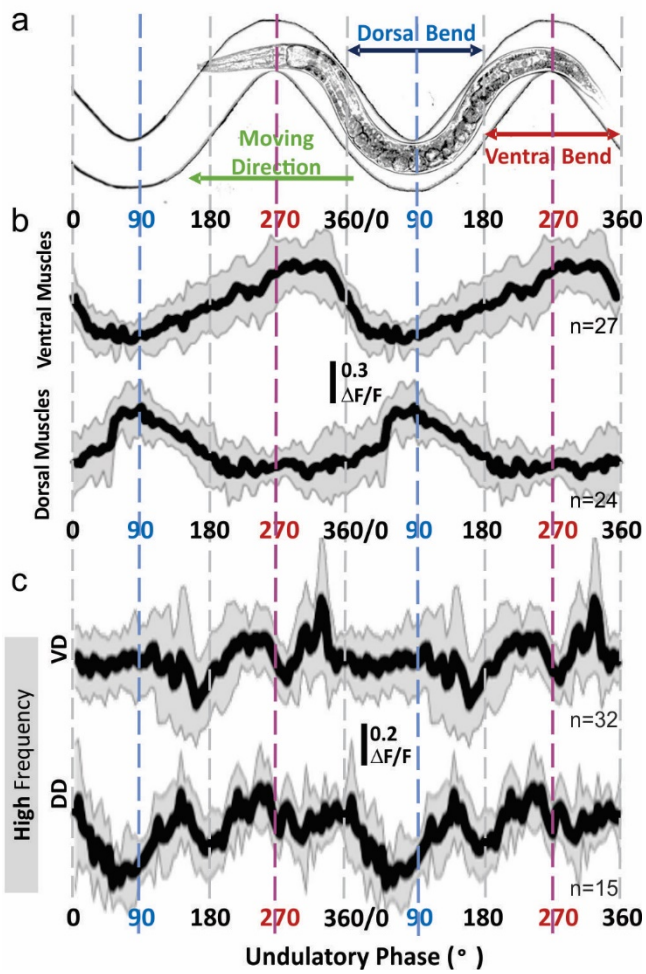


**Figure 7.** Calcium signal patterns of GABAergic motoneurons were different during low and high undulation frequency**.** (a) animals were free to move in sinusoidal microfluidic channels so that the undulatory cycle, including dorsal and ventral bends are fixed in space. (b) Body-wall muscle cells were active at the inside of body bends (e.g., dorsal muscles were active during dorsal bend around 90°). (c) During high undulation frequency crawling, VD showed two troughs around 180° and 270°, and DD around 90° and 180°; only VD showed a sharp increase around 300˚. The sample size (n) indicates the number of analyzed cells. Solid lines and shaded areas in calcium traces are mean and the standard deviation. $\Delta F/F = (F_{top50\%}-F_{BG}) / (\Sigma(F_{top50\%}-F_{BG})/n)$.

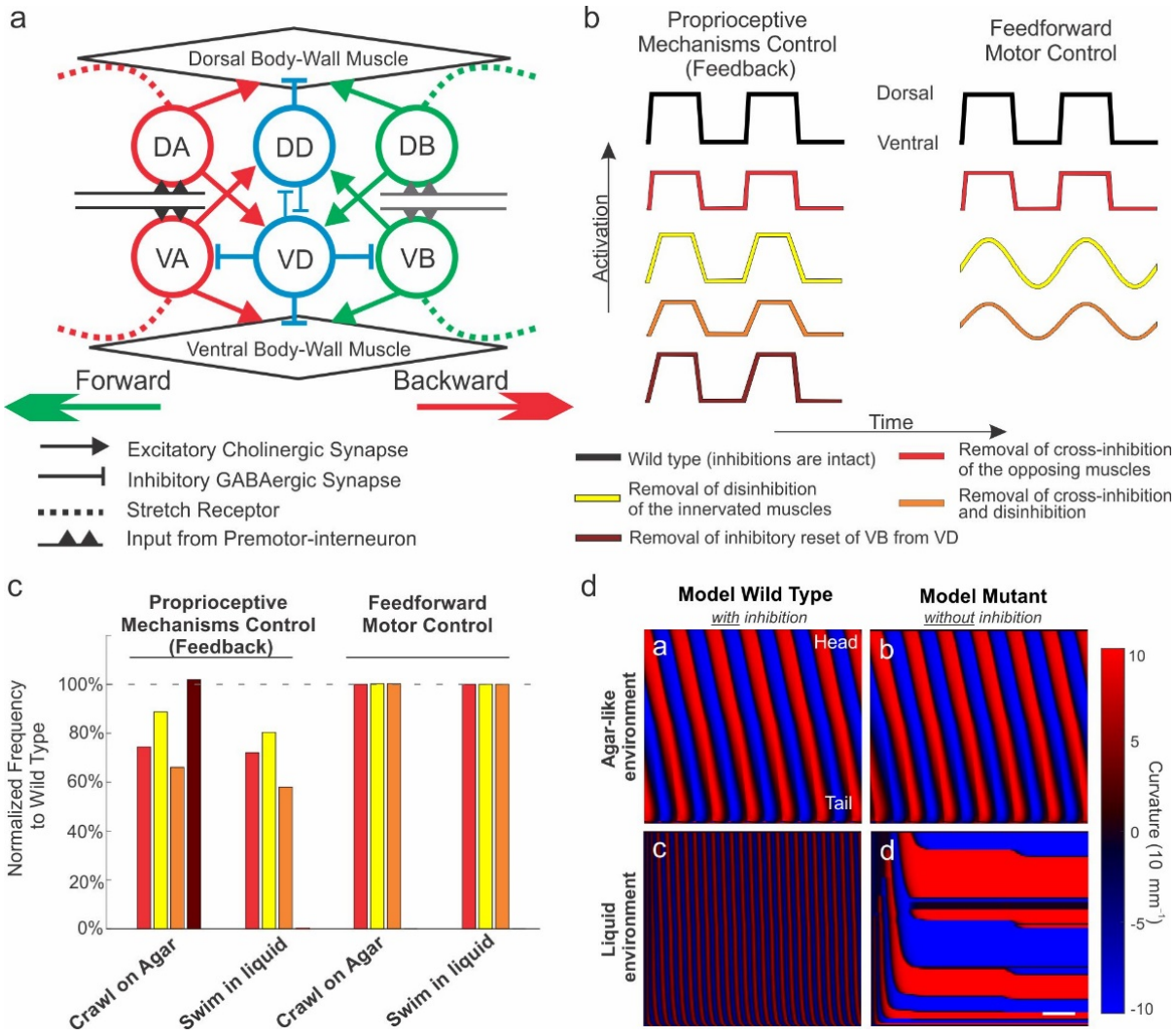
a
Dorsal Body-Wall Muscle
DA
DD
DB
VA
VD
VB
Ventral Body-Wall Muscle
Forward
Backward
Excitatory Cholinergic Synapse
Inhibitory GABAergic Synapse
Stretch Receptor
Input from Premotor-interneuron
b
Proprioceptive Mechanisms Control (Feedback)
Feedforward Motor Control
Dorsal
Ventral
Activation
Time
Wild type (inhibitions are intact)
Removal of disinhibition of the innervated muscles
Removal of inhibitory reset of VB from VD
Removal of cross-inhibition of the opposing muscles
Removal of cross-inhibition and disinhibition
c
Proprioceptive Mechanisms Control (Feedback)
Feedforward Motor Control
Normalized Frequency to Wild Type
100%
80%
60%
40%
20%
0%
Crawl on Agar
Swim in liquid
Crawl on Agar
Swim in liquid
d
Model Wild Type
with inhibition
Model Mutant
without inhibition
Agar-like environment
Liquid environment
a
b
c
d
Head
Tail
Curvature (10 mm⁻¹)
10
5
0
-5
-10

**Figure 8.** Locomotion motor circuit of the *C. elegans* ventral nerve cord has served as a basis for proprioceptive (feedback) mechanisms control computational models. (a) Schematic of locomotion motor circuit of the *C. elegans* in the ventral nerve cord, depicted as a neuromuscular unit, has served as a basis for proprioceptive (feedback) mechanisms control computational models. During forward locomotion, VB and VD (DB and DD) motoneurons innervate ventral (dorsal) muscles and VD motoneurons innervate VB motoneurons. During backward locomotion, A-type cholinergic motoneurons get involved. Stretch receptors (dash lines) transfer the proprioception of local bending and trigger the activation of VB motoneurons during forward locomotion. The non-iterative synapse contact between VD and DD motoneurons (blue thin lines) is not considered in the model. Adapted from Figure 1b of Cohen & Denham (2019). (b) Schematics of the neural activation or muscle input in the proprioceptive control model (left) and feedforward control model (right). The schematic traces indicate muscle input activation status of dorsal and ventral body-wall muscles. When inhibitions are intact in the model wild type (black), the dorsal muscle input (which increases when the trace rises) and the ventral muscle input (which increases when the trace drop down) is antiphase in square shape in proprioceptive feedback and feedforward models. When inhibition(s) is (are) removed, the amplitude or the shape of muscle input traces will be affected. (c) Three hypotheses for the role of inhibition (cross-inhibition of the opposing muscles in red, disinhibition of the innervated muscles in yellow, and inhibitory rest of VB from VD in brown) and one combination (cross-inhibition and disinhibition of muscles in orange) were tested in proprioceptive and feedforward motor control models. In proprioceptive mechanisms control model, these inhibitions play important roles in sustaining rapid undulatory alternations, as in liquid environment the undulation frequency reduced by 100% to 18% of the undulation frequency of wild type. In feedforward motor control model (Berri et al., 2009), only the inhibitory reset of VB from VD resulted in large undulation frequency reduction by 100% from undulation frequency of wild type. The bar figures depict the percentage of undulation frequency of model mutants that normalized to that of model wild type. (d) In proprioceptive mechanisms control model, elimination of inhibitory reset of VB from VD caused failure in generating curvature along the body. The kymograms show curvature dynamics in environments in agar-like environment (ab) and liquid environment (cd) of model wild type animal (ac) and model mutant animal (bd). In agar-like environment, there is no difference with or without the inhibitory reset. In water environment, elimination of the inhibition resulted in failure of curvature generation along the body. Scale bar = 1 s.